

# NeuroTrails: Training with Dynamic Sparse Heads as the Key to Effective Ensembling

Bram Grooten<sup>\*1</sup> Farid Hasanov<sup>\*1,2</sup> Chenxiang Zhang<sup>2</sup> Qiao Xiao<sup>1</sup> Boqian Wu<sup>2,3</sup>  
 Zahra Atashgahi<sup>4</sup> Ghada Sokar<sup>5,1</sup> Shiwei Liu<sup>6,1</sup> Lu Yin<sup>7,1</sup> Elena Mocanu<sup>3</sup>  
 Mykola Pechenizkiy<sup>1</sup> Decebal Constantin Mocanu<sup>2,1</sup>

<sup>1</sup>Eindhoven University of Technology <sup>2</sup>University of Luxembourg <sup>3</sup>University of Twente  
<sup>4</sup>IKEA Netherlands <sup>5</sup>Google DeepMind <sup>6</sup>University of Oxford <sup>7</sup>University of Surrey

## Abstract

Model ensembles have long been a cornerstone for improving generalization and robustness in deep learning. However, their effectiveness often comes at the cost of substantial computational overhead. To address this issue, state-of-the-art methods aim to replicate ensemble-class performance without requiring multiple independently trained networks. Unfortunately, these algorithms often still demand considerable compute at inference. In response to these limitations, we introduce **NeuroTrails**, a sparse multi-head architecture with dynamically evolving topology. This unexplored model-agnostic training paradigm improves ensemble performance while reducing the required resources. We analyze the underlying reason for its effectiveness and observe that the various neural trails induced by dynamic sparsity attain a *Goldilocks zone* of prediction diversity. NeuroTrails displays efficacy with convolutional and transformer-based architectures on computer vision and language tasks. Experiments on ResNet-50/ImageNet, LLaMA-350M/C4, among many others, demonstrate increased accuracy and stronger robustness in zero-shot generalization, while requiring significantly fewer parameters.<sup>1</sup>

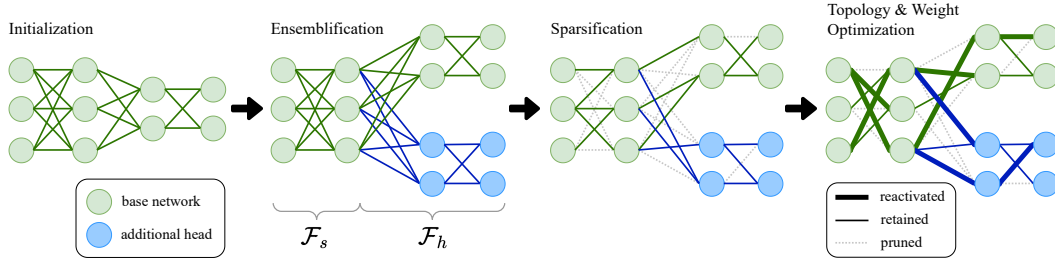


Figure 1: Illustration of NeuroTrails. We divide a network into a shared backbone  $\mathcal{F}_s$  and multiple independent heads  $\mathcal{F}_h$ . Weights are initially pruned at random to a target sparsity ratio. Finally, the network topology is repeatedly refined through dynamic sparse training. The resulting sparse multi-head architecture achieves better performance than a full ensemble while using fewer resources.

## 1 Introduction

The idea of combining the outputs of multiple models to produce a stronger predictor has been around for a long time, with foundational works on stacking linear models (Beyer, 1981; Wolpert, 1992), bagging (Breiman, 1996) and boosting (Freund and Schapire, 1997)

<sup>\*</sup>Equal contribution. Corresponding authors: b.grooten@tue.nl and f.e.o.hasanov@tue.nl.

<sup>1</sup>Our open-source code is available at <https://github.com/bramgrooten/neurotrails>.

establishing the efficacy of this approach. Following these early developments, ensembling has proven to be a powerful technique in deep learning to increase accuracy, robustness, and generalization performance (Hansen and Salamon, 1990; Maclin and Opitz, 2011; Zhou, 2012). A common approach involves training multiple deep neural networks independently and averaging their predictions at inference (Zhou, 2012). Random initialization allows ensemble models to explore various local optima, diversifying their predictions (Fort et al., 2020). However, the huge increase in required compute is a significant disadvantage.

Multiple works have attempted to reduce this overhead by, for example, factorizing weight matrices (Wen et al., 2020), network distillation (Hinton et al., 2015), or with a Multi-Input Multi-Output configuration (MIMO) (Havasi et al., 2021), usually reducing the number of parameters of an ensemble to be approximately similar to a single model. An alternative approach to reducing the parameter counts of neural networks lies in the extensive field of pruning (Frankle and Carbin, 2019; Lee et al., 2018; Wang et al., 2020) and dynamic sparse training (Mocanu et al., 2018; Evci et al., 2020). Various studies leverage these methods to address the complexity challenges associated with ensembles (Liu et al., 2022; Whitaker and Whitley, 2022).

In this paper, we approach ensembles from the perspective of TreeNet architectures (Lee et al., 2015). These are structures that share the early layers of neural networks, while retaining as many heads as a corresponding ensemble. While TreeNet’s shared backbone reduces the parameter count, the performance may not always match a full ensemble, as the heads often fail to achieve enough separation in prediction diversity.

To resolve this, we introduce **NeuroTrails**, a novel training paradigm enabling ensemble models to share early backbone layers while forming diverse independent trails further in the network, see Figure 1. We train the multi-head model using dynamic sparse training, which allows NeuroTrails to adapt the network topology over time. By tuning the backbone length, the resulting model attains a *Goldilocks zone* of prediction diversity—neither too little nor too much (Section 5.2). Furthermore, the sparsity enables parameter reduction, directly translating to inference speedups (Section 5.4).

NeuroTrails is model-agnostic, outperforming ensembles built from both convolutional networks (ResNet-50, Wide-ResNet28-10) and transformer models (LLaMA-130M, LLaMA-350M). It surpasses them on computer vision and language benchmarks such as CIFAR-100, ImageNet, and the Colossal Clean Crawled Corpus, see Table 1. Additionally, NeuroTrails displays strong zero-shot generalization to out-of-distribution images and downstream language tasks.

In summary, our contributions are:

- We introduce NeuroTrails, a novel training paradigm improving neural network ensembles through two key mechanisms: shared early layers and dynamic sparse training.
- We validate our model-agnostic approach with extensive vision and language experiments on common benchmarks, showing consistent improvements over TreeNet and full ensembles.
- We provide deeper analysis on prediction diversity, real-time speedups, and key design factors—including the optimal splitting point, ensemble size, and sparsity ratio.

## 2 Preliminaries

### 2.1 Ensembling

Combining the strength of multiple models in an ensemble is widely studied in the literature, and has been shown to reduce variance and improve generalization (Hansen and Salamon, 1990). Ensembles can be used for uncertainty estimation (Lakshminarayanan et al., 2017), leading to more calibrated probability estimates, covering a larger portion of the problem space, bridging representation gaps left by individual models (Dietterich, 2000; Zhou, 2012). However, the additional computational cost in training and inference of neural network ensembles severely limits their scope of application (Gomes et al., 2017; Dietterich, 2000).

Table 1: NeuroTrails achieves higher ImageNet accuracy and lower C4 perplexity.

Method	ResNet-50/ImageNet Accuracy ( $\uparrow$ )	LLaMA-350M/C4 Perplexity ( $\downarrow$ )
Single Network	76.1	22.8
Full Ensemble	77.5	21.3
<b>NeuroTrails</b>	<b>78.1</b>	<b>20.7</b>

Random initialization allows ensemble models to explore various local optima, diversifying their predictions (Fort et al., 2020). However, the huge increase in required compute is a significant disadvantage.

## 2.2 Sparsity

The sparsification of neural networks has been a prevalent resolution to ease this computational burden (LeCun et al., 1989; Frankle and Carbin, 2019; Evci et al., 2020). Sparsifying a network involves removing a certain fraction of its parameters to create a lightweight model. Let an  $n \times k$  dense layer be the weighted digraph  $G = (V, E_{\text{dense}}, \theta)$  where  $V = V_{\text{in}} \cup V_{\text{out}}$  is the set of neurons,  $E_{\text{dense}} = V_{\text{in}} \times V_{\text{out}}$  the set of potential edges, and  $\theta \in \mathbb{R}^{nk}$  the corresponding weight matrix. A binary mask  $\mathbf{m} \in \{0, 1\}^{nk}$  selects the active edge set  $E = \{e_i \mid m_i = 1\}$ , producing the sparse weight matrix  $\theta \odot \mathbf{m}$ . The *sparsity ratio*  $S = 1 - \|\mathbf{m}\|_0/nk \in [0, 1]$  is the fraction of edges removed.

**Pruning.** Pruning methods generally involve training a *dense* network to convergence, then selecting a mask  $\mathbf{m}$  with the desired sparsity, classifying these algorithms as **dense-to-sparse**. The process ranks each weight  $\theta_i$  with an importance score  $s_i$ , keeping the top  $(1 - S)nk$  entries. Typically used scores are magnitude  $s_i^{\text{mag}} = |\theta_i|$ , first-order  $s_i^{(1)} = |\theta_i g_i|$  with  $g_i = \partial \mathcal{L} / \partial \theta_i$  (Mozer and Smolensky, 1988), and second-order  $s_i^{(2)} = \frac{1}{2} \theta_i^2 H_{ii}$  with  $H_{ii} = \partial^2 \mathcal{L} / \partial \theta_i^2$  (LeCun et al., 1989). A short finetuning pass can restore accuracy after pruning (Han et al., 2015). See Appendix B for further background and lottery-ticket variants.

**Sparse Training.** Training neural networks with a sparse structure throughout the entire training process is the counterpart of pruning, depicting a **sparse-to-sparse** paradigm. In *static* sparse training, the network topology is fixed, making it very sensitive to the initial choice of  $\mathbf{m}$ . *Dynamic* sparse training (DST) solves this issue, enabling the sparse topology to be adaptive. Popular algorithms that exemplify this methodology are Sparse Evolutionary Training (SET) (Mocanu et al., 2018) and Rigged Lottery Tickets (RigL) (Evci et al., 2020). SET starts with a sparsely connected neural network and iteratively updates its structure  $\mathbf{m}$  over fixed intervals  $\Delta T$ . At each topology update, a drop fraction  $p$  of the active weights with the smallest magnitude  $|\theta_i|$  is pruned, after which an equal number of inactive weights are regrown uniformly at random. RigL uses gradients of inactive connections to guide regrowth, always selecting the highest absolute gradients  $|g_i|$  as most promising.

## 3 NeuroTrails

We introduce NeuroTrails, a novel training paradigm to enhance the performance of neural network ensembles, while reducing their parameter complexity (see Figure 1). The method is model-agnostic and can be applied to any architecture. See Appendix G for a concise pseudocode overview.

**Architecture split.** Let the base network  $\mathcal{F}$  be a composition of  $L$  blocks

$$\mathcal{F}(x; \theta) = f_L(f_{L-1}(\cdots f_1(x; \theta_1) \cdots; \theta_{L-1}); \theta_L)$$

where a block is a collection of neural network layers, such as a residual or transformer block. We choose a split index  $1 \leq \ell \leq L$  and partition into

$$\mathcal{F}_s(x; \theta_s) = f_\ell \circ \cdots \circ f_1, \quad \mathcal{F}_h(x; \theta_h) = f_L \circ \cdots \circ f_{\ell+1}.$$

We instantiate  $M$  independent heads  $\mathcal{F}_h^{(i)}$  ( $i = 1, \dots, M$ ), each with separately initialized weights  $\theta_h^{(i)}$  and sparse mask  $\mathbf{m}_h^{(i)}$ . These unique initial conditions seed distinct “neural trails”—deep, long-range connectivity paths that give the multi-head network its diversity. The shared trunk  $\mathcal{F}_s$  likewise carries a mask  $\mathbf{m}_s$ . We analyze the ideal backbone length  $\ell$  in Section 5.1, and investigate the effect of different sparsity ratios  $S$  in Appendix I. In the remainder of this paper, we will denote the number of blocks in the backbone and heads by  $|\mathcal{F}_s| = \ell$  and  $|\mathcal{F}_h| = L - \ell$ , respectively.

**Training.** On a minibatch  $(x, y)$ , we compute each head’s logits

$$\hat{y}^{(i)} = \mathcal{F}_h^{(i)}(\mathcal{F}_s(x; \theta_s); \theta_h^{(i)}).$$

Individual losses  $\mathcal{L}_i$  for each head  $i$  are calculated and averaged to form the composite loss,

$$\mathcal{L}(\Theta) = \frac{1}{M} \sum_{i=1}^M \mathcal{L}_i(\hat{y}^{(i)}, y), \quad \Theta = (\theta_s, \theta_h^{(1)}, \dots, \theta_h^{(M)}),$$

which is used to update all active parameters through a masked version of stochastic gradient descent (Robbins and Monro, 1951) or Adam (Kingma and Ba, 2015). Every  $\Delta T$  steps, each component (shared or head  $i$ ), performs a topology update through dynamic sparse training. This process consists of (1) layerwise pruning of  $p$  weights, and (2) reinitializing an equal number  $p$  previously inactive connections, thereby maintaining a constant density  $\|\mathbf{m}\|_0/nk$  while exploring new sparse trails.

In computer vision experiments, we reactivate weights with RigL (Evci et al., 2020) and prune by standard magnitude  $|\theta_i|$ , as recommended by Nowak et al. (2023). We use the Erdős–Rényi (ER) approach (Mocanu et al., 2018; Evci et al., 2020) to distribute the global sparsity  $S$  into layerwise sparsity ratios. ER has been shown to yield superior performance over simply setting each layer’s sparsity to  $S$ , i.e., uniform sparsity (Liu et al., 2023). In a nutshell, ER assigns higher sparsity ratios to larger layers. See Appendix B for additional information.

For language modeling, we likewise use ER, but leave attention projections dense while sparsifying all other layers. Furthermore, we also use RigL for growth, but we prune using *soft magnitude*, shown to work well for LLMs by Zhang et al. (2025). In this procedure, a weight’s absolute value determines a *probability* of being pruned, instead of simply pruning the smallest weights.

Dense models tend to overfit once training is prolonged, whereas sparse networks keep improving as they are still refining both weights and topology (Liu et al., 2021b). According to the schedules of Evci et al. (2020), we extend the training of sparse variants by at most  $1/(1-S)$ , always keeping the total number of floating-point operations (FLOPs) for training below those of their dense counterparts. Exact number of epochs—or updates in the case of language modeling—appear in Appendix E.

**Inference.** During inference, the final prediction is computed through soft voting, averaging logits across all ensemble members:

$$\bar{y} = \frac{1}{M} \sum_{i=1}^M \mathcal{F}_h^{(i)}(F_s(x; \theta_s); \theta_h^{(i)}).$$

The shared backbone  $F_s(x; \theta_s)$  forward pass naturally only needs to be computed once. NeuroTrails ensures that while ensemble members share early feature extractors, the heads develop distinct predictive pathways through sparse connectivity patterns, thereby stimulating diversity.

Table 2: Performance on **CIFAR-100** with Wide-ResNet28-10 as the base. NeuroTrails and TreeNet have 8 blocks in the heads, with 4 remaining blocks in the shared backbone. Results marked with \* are from Havasi et al. (2021), \*\* from Liu et al. (2022), and \*\*\* from Lee and Lee (2024).

Name	Accuracy ( $\uparrow$ )	NLL ( $\downarrow$ )	ECE ( $\downarrow$ )	Train FLOPs ( $\downarrow$ )	Infer. FLOPs ( $\downarrow$ )
Single Dense *	79.8	0.875	0.086	3.6e17	10.5e9
MIMO ( $M = 3$ ) *	82.0	0.690	0.022	1.00×	1.00×
EDST Ensemble ( $M = 7$ ) ( $S = 0.9$ ) **	82.6	0.653	0.036	<b>0.57×</b>	1.17×
DST Ensemble ( $M = 3$ ) ( $S = 0.8$ ) **	83.3	<b>0.623</b>	<b>0.018</b>	1.01×	1.01×
Batch Ensemble ( $M = 4$ ) *	81.5	0.740	0.056	1.10×	1.10×
NFE ( $M = 3$ ) ***	83.5	0.658	0.061	1.02×	1.02×
TreeNet ( $M = 3$ )	83.2	0.673	0.052	2.91×	2.91×
Full Ensemble ( $M = 3$ )	83.3	0.663	0.042	3.00×	3.00×
NeuroTrails ( $M = 3$ ) ( $S = 0.8$ )	83.8	0.681	0.044	0.85×	0.47×
NeuroTrails ( $M = 5$ ) ( $S = 0.9$ )	<b>83.9</b>	0.675	0.041	0.67×	<b>0.37×</b>

Table 3: Performance on **ImageNet** with ResNet-50 as the baseline model. NeuroTrails and TreeNet have 10 blocks in their multi-head structure, with 6 remaining blocks in the shared backbone. Results marked with \* are from Havasi et al. (2021) and \*\* from Liu et al. (2022).

Name	Accuracy ( $\uparrow$ )	NLL ( $\downarrow$ )	ECE ( $\downarrow$ )	Train FLOPs ( $\downarrow$ )	Infer. FLOPs ( $\downarrow$ )
Single Dense *	76.1	0.943	0.039	4.8e18	8.2e9
MIMO ( $M = 2$ ) ( $\rho = 0.6$ ) *	77.5	0.887	0.037	1.00×	1.00×
EDST Ensemble ( $M = 4$ ) ( $S = 0.8$ ) **	77.7	0.935	0.064	<b>0.87×</b>	1.78×
DST Ensemble ( $M = 2$ ) ( $S = 0.8$ ) **	<b>78.3</b>	0.914	0.060	1.12×	1.12×
Batch Ensemble ( $M = 4$ ) *	76.7	0.944	0.049	1.10×	1.10×
TreeNet ( $M = 3$ )	78.1	0.886	0.053	2.91×	2.91×
Full Ensemble ( $M = 4$ ) *	77.5	0.877	<b>0.031</b>	4.00×	4.00×
NeuroTrails ( $M = 3$ ) ( $S = 0.7$ )	78.1	<b>0.861</b>	0.038	1.10×	<b>0.67×</b>

## 4 Experiments and Results

We compare our methods against a single model, a full ensemble, and various state-of-the-art efficient ensemble methods in the literature, including MIMO (Havasi et al., 2021), TreeNet (Lee et al., 2015), Batch Ensemble (Wen et al., 2020), as well as DST and EDST ensembles (Liu et al., 2022). See Section 6 for detailed descriptions of these baselines. All architectures use the following base models: Wide-ResNet28-10 on CIFAR-100, ResNet-50 on ImageNet, and LLaMA-130M/350M on C4. Details on the training regime and hyperparameters are shared in Appendix E.

For computer vision experiments, we report the mean test accuracy, negative log-likelihood (NLL), and expected calibration error (ECE). In language modeling, our main metric is perplexity on the C4 validation set. We include the required number of FLOPs for training and inference. Next to the name of the model, we indicate the ensemble size (or number of heads)  $M$  and sparsity ratio  $S$ . See Appendix F for further details on the metrics.

### 4.1 Results on Computer Vision

As shown in Tables 2 and 3, NeuroTrails demonstrates strong performance both on CIFAR-100 and ImageNet, while using significantly fewer FLOPs at inference time. We present additional results on Tiny-ImageNet in Appendix H. The low FLOPs required at inference are crucial, making NeuroTrails a compelling choice for deployment in resource-constrained environments. See Section 5.4 for the real-time speedups that are already possible.

**Robustness against Corruptions.** To test NeuroTrails for its zero-shot generalization capability, we evaluate its robustness to corrupted ImageNet samples. The benchmark ImageNet-C (Hendrycks and Dietterich, 2019) consists of various corruption types applied at five severity levels. Furthermore, we test baselines on ImageNet-Sketch (Wang et al., 2019), a collection of black-and-white sketched illustrations, assessing the model’s ability to extrapolate to out-of-domain data.

Our results in Figure 2 show that NeuroTrails consistently outperforms the full ensemble across all corruption levels. On ImageNet-Sketch, our method similarly shows significantly better generalization ability, achieving +3.02 and +0.92 percentage points over a single model and a full ensemble, respectively.

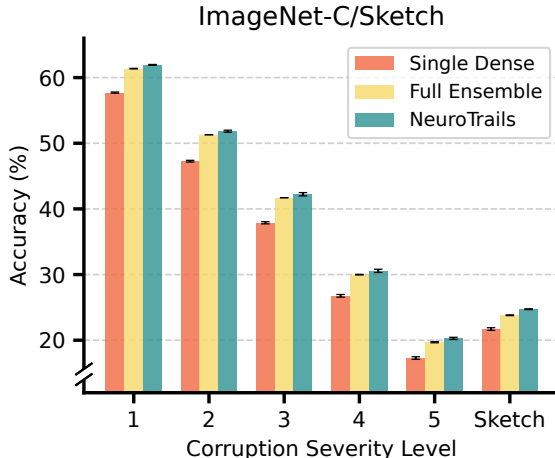


Figure 2: Testing zero-shot generalization ability on corrupted ImageNet samples and out-of-domain sketches. NeuroTrails outperforms a full ensemble in robustness, despite requiring a fraction of its FLOPs.

### 4.2 Results on Language Modeling

We pretrain variants of LLaMA-130M and LLaMA-350M on the *Colossal Clean Crawled Corpus* (C4) text dataset (Raffel et al., 2020). Motivated by the work of Wu et al. (2025), we use a low sparsity ratio in these experiments, but maintain the adaptive nature of dynamic sparse training. The results in Table 4 show that NeuroTrails performs strongly on transformer architectures, achieving the best validation perplexity. Despite using a lower sparsity ratio in the language domain, our algorithm yields a lightweight model with lower inference FLOPs than both TreeNet and the full ensemble. A natural question is whether scaling a single dense model would be more effective than ensembling. Appendix H shows that, given the same parameter budget, NeuroTrails still achieves lower perplexity.

**Evaluation on Downstream Tasks.** We test our pretrained LLaMA-350M models for zero-shot generalization to multiple downstream tasks. The results in Table 5 compare model accuracy across seven benchmarks: MMLU (Hendrycks et al., 2021), BoolQ (Clark et al., 2019), ARC (Clark et al., 2018), PIQA (Bisk et al., 2019), Hellaswag (Zellers et al., 2019), OpenbookQA (Mihaylov et al.,

Table 4: Pretraining performance on the **C4** dataset with LLaMA-130M/350M as the baseline model. NeuroTrails and TreeNet use  $\frac{2}{3}$  of the transformer blocks in the heads, with  $\frac{1}{3}$  in the backbone.

Name	Perplexity ( $\downarrow$ )	Training FLOPs ( $\downarrow$ )	Inference FLOPs ( $\downarrow$ )
<i>LLaMA-130M</i>			
Single Dense	29.06	3.5e18	2.2e11
TreeNet ( $M = 3$ )	26.46	<b>2.21×</b>	2.21×
Full Ensemble ( $M = 3$ )	26.88	3.00×	3.00×
NeuroTrails ( $M = 3$ ) ( $S = 0.1$ )	<b>26.00</b>	<b>2.21×</b>	<b>1.99×</b>
<i>LLaMA-350M</i>			
Single Dense	22.80	4.2e19	6.9e11
TreeNet ( $M = 3$ )	21.06	<b>2.27×</b>	2.27×
Full Ensemble ( $M = 3$ )	21.25	3.00×	3.00×
NeuroTrails ( $M = 3$ ) ( $S = 0.1$ )	<b>20.70</b>	<b>2.27×</b>	<b>2.04×</b>

Table 5: Zero-shot accuracy ( $\uparrow$ ) of various LLaMA-350M models across seven downstream tasks.

Model	MMLU	BoolQ	ARC	PIQA	Hellaswag	OBQA	WinoGrande	Avg.
Single Dense	22.92	58.47	40.24	62.51	28.31	13.60	<b>52.49</b>	39.79
TreeNet ( $M = 3$ )	<b>22.97</b>	58.65	40.40	62.95	<b>28.45</b>	15.00	51.30	39.96
Full Ensemble ( $M = 3$ )	<b>22.97</b>	58.23	40.36	62.68	28.18	14.40	51.70	39.78
NeuroTrails ( $M = 3$ ) ( $S = 0.1$ )	22.92	<b>60.49</b>	<b>41.71</b>	<b>63.28</b>	28.43	<b>15.80</b>	50.51	<b>40.45</b>

2018), and WinoGrande (Sakaguchi et al., 2019). These tasks span multiple domains including common sense reasoning, multiple choice question answering, and scientific knowledge. NeuroTrails achieves the highest average accuracy, suggesting that it offers improved generalization and robustness across a wide range of language tasks.

## 5 Analysis

In this section, we explore various design choices for NeuroTrails. All results reported here were obtained using Wide-ResNet28-10 as the baseline model, evaluated on CIFAR-100, and present the mean and standard deviation over 3 independent seeds.

### 5.1 Backbone Length

An essential hyperparameter of NeuroTrails is the optimal split index  $l$ . The ideal architecture may depend on both the sparsity ratio  $S$  and the number of heads  $M$ ; our analysis focuses on the configuration with 80% sparsity and 3 heads. In addition, we examine different sparsification methods on the same plot.

As detailed in Section 3, we split the architecture between blocks, where each block in Wide-ResNet28-10 consists of two convolutional layers, two batch normalization layers and a residual connection. The base network Wide-ResNet28-10 has 12 blocks in total, so we can vary the backbone length across this depth. The results shown in Figure 3 reveal that performance is maximized most efficiently with a split point at 8 blocks per head. This architecture consists of

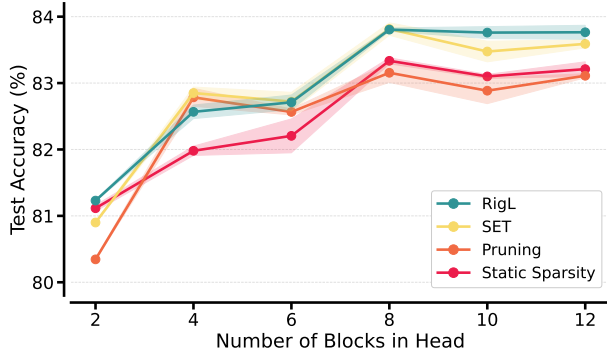


Figure 3: Performance of NeuroTrails models with varying backbone sizes and sparsification methods (CIFAR-100 with Wide-ResNet28-10). **Backbone Length:** The most *effective* (optimizing accuracy and efficiency<sup>2</sup>) backbone length appears around  $\frac{1}{3}$  of the network, meaning  $\frac{8}{12}$  blocks in head. **Sparsification:** The dynamic sparse training algorithms RigL and SET demonstrate superior performance, confirming DST as the optimal approach.

<sup>2</sup>Minimizing the blocks per head increases efficiency, as NeuroTrails then contains fewer parameters.

Table 6: Comparison of prediction disagreement (PD) and model performance on CIFAR-100 using Wide-ResNet28-10. NeuroTrails achieves peak accuracy at  $|\mathcal{F}_h| = 8$ , with lower PD than configurations using more head blocks. This suggests that optimal performance lies in a *Goldilocks zone* where PD is neither too low nor too high.

Model	Blocks in head	PD (%)	Acc. (%)
NeuroTrails	2	2.9	80.89
	4	11.2	82.85
	6	12.4	82.71
	8	14.6	<b>83.81</b>
	10	15.3	83.47
	12	16.0	83.59
Full Ensemble	–	15.4	83.62

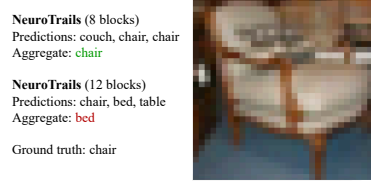


Figure 4: Example of a CIFAR-100 test-set image where too much prediction diversity between heads degrades performance. NeuroTrails with 8 blocks in each head seems to get the amount of diversity *just right*. For more illustrations of predictions with overly large diversity, see [Appendix K](#).

four shared backbone blocks ( $|\mathcal{F}_s| = 12 - 8 = 4$ ) and eight blocks for each of the independent heads ( $|\mathcal{F}_h| = 8$ ), resulting in approximately one-third of the network serving as the shared backbone. The different sparsification methods used have varying performance. However, the dynamic nature of RigL and SET helps them to consistently surpass static sparse training and standard one-time pruning.

## 5.2 Prediction Diversity

In this section, we analyze the prediction diversity of NeuroTrails. Although numerous metrics exist for quantifying diversity ([Kuncheva and Whitaker, 2003](#)), we adopt Prediction Disagreement (PD), one of the most widely used. PD is defined as the proportion of test samples where ensemble members produce conflicting predictions ([Skalak, 1996](#)).

Analysis of PD patterns in [Table 6](#) reveals a monotonic increase in inter-head disagreement as the proportion of the NeuroTrails architecture allocated to independent heads grows. This observation aligns with intuition: As a larger portion of the network is dedicated to the heads, the extra head-only layers let each branch specialize, so their outputs drift further from the initially shared representation. A surprising finding emerges from our most accurate configuration with  $|\mathcal{F}_h| = 8$ : This model exhibits *lower* prediction disagreement between heads (14.6) compared to a full ensemble (15.4) and configurations with more blocks in the heads (up to 16.0), while being superior in performance.

This observation points to the existence of an optimal disagreement threshold, which we refer to as the *PD Goldilocks zone* (due to the amount being ‘just right’). Beyond this threshold, excessive prediction diversity among ensemble members begins to degrade model performance. When heads make significantly divergent predictions for the same input, they cease to complement each other and instead compete, negating their contributions. This insight highlights that, while a certain level of diversity is beneficial in ensemble learning, excessive diversity can be detrimental, see [Figure 4](#). Achieving the right balance between diversity and consensus is essential to maximize ensemble performance. For further analysis on this issue, see [Appendix K](#).

**Prediction Disagreement over Time.** We observe in [Figure 5](#) that PD decreases throughout training as accuracy is growing for the NeuroTrails model ( $M = 3, S = 0.8$ ). At the start of the training, PD is relatively high (30 ~ 40%) and continues to decrease before reaching a steady value of approximately 14.6% at the end of the training. The relationship between PD and accuracy exhibits a notable negative correlation, particularly evident at transition points of the stepwise learning rate decay. This analysis highlights that while high diversity between heads does not guarantee better performance, low diversity similarly limits ensemble benefits.

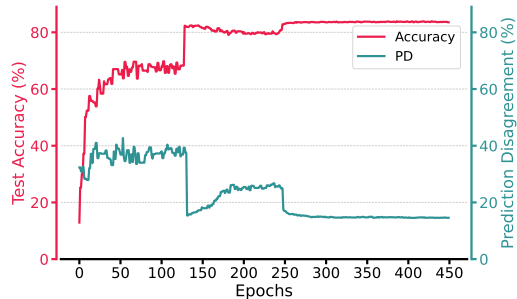


Figure 5: Accuracy and Prediction Disagreement throughout training for a NeuroTrails model on CIFAR-100, showing an inverse trend.

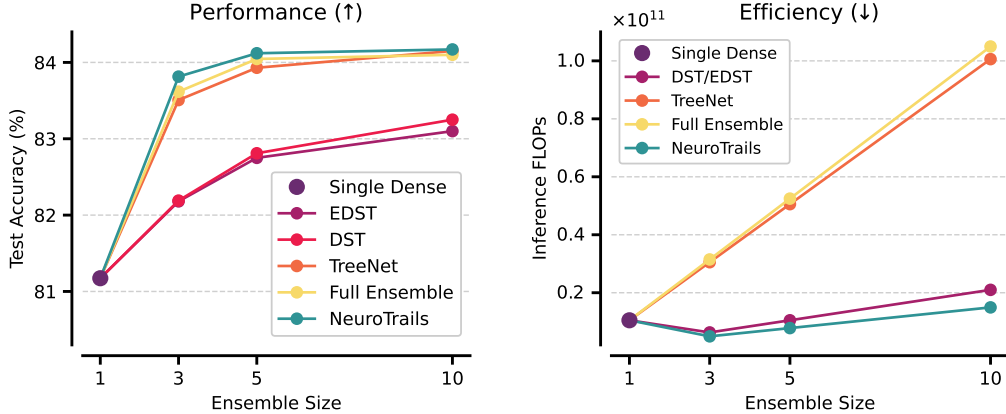


Figure 6: Effect of the ensemble size on CIFAR-100 with Wide-ResNet28-10. NeuroTrails achieves higher accuracy than a full ensemble (**left**) while consuming only a fraction of the FLOPs (**right**).

### 5.3 Ensemble Size

We analyze the impact of ensemble size  $M$  on performance and efficiency. Single networks and standard ensembles are fully dense, while NeuroTrails uses 80% sparsity and  $|\mathcal{F}_h| = 8$  across all experiments in this section. The results are summarized in Figure 6. Both traditional ensembles and NeuroTrails show significant accuracy gains as the ensemble size increases from 1 to 10, with NeuroTrails consistently outperforming the baselines across all sizes. The most substantial improvements occur between sizes 1 and 3, followed by diminishing returns.

The trade-offs are further illustrated in the right plot of Figure 6. Due to its high sparsity, NeuroTrails incurs significantly lower computational costs, scaling more efficiently with ensemble size. These gains could be further amplified—e.g., a 5-head NeuroTrails can support 90% sparsity without a drop in performance on CIFAR-100 (see Table 2)—while larger ensembles may enable even greater sparsity. Exploring such configurations is a promising avenue for future work.

### 5.4 Inference Speedup

While FLOPs reduction is a widely used proxy for model efficiency, achieving real-world speedups often hinges on hardware compatibility and software execution paths. Recent hardware advances, such as the Cerebras CS-2 system, have shown that unstructured sparsity can translate into substantial runtime performance gains, even on GPU-class accelerators (Cerebras, 2024).

In parallel, software frameworks such as DeepSparse already deliver substantial inference-time performance improvements on commodity CPU hardware (NeuralMagic, 2021). In our experiments using DeepSparse, we observe that NeuroTrails models significantly outperform full ensembles in terms of practical efficiency, see Table 7. While dense ensembles suffer from considerable reductions in throughput and increased latency as the ensemble size grows, NeuroTrails maintains high efficiency. For example, NeuroTrails with a sparsity ratio of 95% achieves 52.05 images per second, approaching the throughput of a single dense model. These results position NeuroTrails as a compelling solution for deployment on smartphones or other edge devices, where resources are constrained and GPUs are often unavailable. Software frameworks for unstructured sparsity on GPUs are likewise on the horizon—details appear in Appendix J.

Table 7: NeuroTrails achieves real-time inference speedups with DeepSparse on CPU hardware.

Model on CIFAR-100	Throughput ↑ (items/sec)	Latency Mean ↓ (ms/batch)	Accuracy ↑ (%)
Single Dense	55.81	17.90 ± 0.72	79.80 ± 0.10
NeuroTrails ( $M=3, S=0.8$ )	26.46	37.78 ± 1.33	<b>83.84 ± 0.11</b>
NeuroTrails ( $M=3, S=0.95$ )	52.05	19.20 ± 2.45	83.05 ± 0.12
NeuroTrails ( $M=3, S=0.99$ )	<b>68.64</b>	<b>14.55 ± 0.75</b>	80.20 ± 0.08
Full Ensemble ( $M=3$ )	18.65	53.61 ± 2.98	83.45 ± 0.34

Table 8: Comparison between baselines across key ensembling desiderata. NeuroTrails exhibits a unique combination. Symbols: ✓ = meets criterion, ✗ = does not meet, ~ = partially.

Method	Prediction Diversity	Efficient Inference	Low Training FLOPs	High Performance
Single Dense	✗	✓	✓	✗
MIMO	✓	~	✓	~
EDST Ensemble	~	~	✓	~
DST Ensemble	✓	~	~	~
TreeNet	~	~	✓	~
Full Ensemble	✓	✗	✗	✓
<b>NeuroTrails</b>	✓	✓	✓	✓

## 6 Related Work

In deep learning, multiple attempts have been made to achieve ensemble-level performance while attaining significant reductions in parameter count and FLOPs. In Table 8 we provide a direct comparison between NeuroTrails and the varying baselines used in our experiments, indicating that our method presents a novel combination of characteristics. We focus on the most related methods in this section; Appendix B expands on additional topics—including Mixture-of-Experts, the Lottery Ticket Hypothesis, and further sparse training studies.

Batch Ensemble (Wen et al., 2020) introduced an efficient ensemble approach by decomposing the ensemble members into a shared matrix and rank-one personalized matrices, achieving near-single network computational costs. Multi-Input Multi-Output Ensembles (MIMO) (Havasi et al., 2021) subsequently improved on this method by ensembling only input and output layers, demonstrating enhanced performance across ensemble architectures. In MIMO, the full original network is always used as the main structure, while adding heads as additional layers at the input and output ends. NeuroTrails differs in this regard, as it only splits into heads on the output side. Furthermore, NeuroTrails has the ability to flexibly configure where our backbone splits into multiple heads, not needing to keep the full original network intact.

In TreeNets, Lee et al. (2015) propose sharing early layers for ensembles. We enhance this approach with two major components: (1) by incorporating dynamic sparse training, which fosters greater diversity and independence among neural pathways throughout the multi-headed network, significantly reducing the number of parameters and FLOPs required, particularly during inference; and (2) by splitting the backbone based on layer-based blocks rather than individual layers, preserving the structural integrity inherent in widely-used architectures such as ResNets (He et al., 2016) and Transformers (Vaswani et al., 2017).

Liu et al. (2022) use dynamic sparse training for ensembles, but do not use a multi-headed network structure. In the DST ensemble approach, independent sparse neural networks are trained from scratch, while their Efficient-DST (EDST) method creates an ensemble from a single network by using distinct model checkpoints throughout training.

## 7 Conclusion

We introduce **NeuroTrails**, a novel training paradigm that is straightforward to integrate into various neural network architectures and yields significant performance improvements. The methodology splits a network into multiple sparse heads, optimizing their topology through dynamic sparse training. Our experiments demonstrate that comprehensive ensembling of all layers is not a necessary condition to achieve optimal performance. In all neural network architectures we experimented on, early-stage feature extraction is more effectively handled through a single shared backbone.

Dynamic sparse training plays a key role in enhancing the performance of a multi-head network, creating distinct neural trails which seem to induce an amount of prediction diversity that is *just right*, i.e., in the PD Goldilocks zone. Furthermore, the resulting architecture of NeuroTrails requires fewer parameters and FLOPs, boosting its efficiency. The lack of widely available sparsity-aware hardware is our main limitation, but there is ongoing work in this direction. Expanding NeuroTrails to even more learning paradigms and network types represents a promising direction for future research.

## Acknowledgments and Disclosure of Funding

We thank Hojoon Lee and Mickey Beurskens for providing valuable feedback on early versions of the paper. Bram Grooten is supported by the AMADeuS project of the Open Technology Programme (project number 18489), which is partly financed by the Dutch Research Council (NWO). This research used the Dutch national e-infrastructure with the support of the SURF Cooperative, using grant number EINF-12945. Farid Hasanov is partly funded by EU Horizon Synergies project 101146542. Part of the experiments were performed on the Luxembourg national supercomputer MeluXina. We gratefully acknowledge the LuxProvide teams for their expert support. Furthermore, some of the experiments presented in this paper were carried out using the HPC facilities of the University of Luxembourg (Varrette et al., 2022). Elena Mocanu is partly supported by the Modular Integrated Sustainable Datacenter (MISD) project funded by the Dutch Ministry of Economic Affairs and Climate under the European Important Projects of Common European Interest - Cloud Infrastructure and Services (IPCEI-CIS) program for 2024–2029.

## References

- Yue Bai, Huan Wang, Zhiqiang Tao, Kunpeng Li, and Yun Fu. Dual Lottery Ticket Hypothesis. In *The Tenth International Conference on Learning Representations, ICLR 2022, Virtual Event, April 25-29, 2022*. OpenReview.net, 2022. URL: <https://arxiv.org/abs/2203.04248>. (Cited on page 17)
- Guillaume Bellec, David Kappel, Wolfgang Maass, and Robert Legenstein. Deep Rewiring: Training very sparse deep networks. *CoRR*, abs/1711.05136, 2017. URL: <https://arxiv.org/abs/1711.05136>. (Cited on page 18)
- H. Beyer. Exploratory Data Analysis. *Biometrical Journal*, 23(4):413–414, January 1981. ISSN 1521-4036. URL: <https://doi.org/10.1002/bimj.4710230408>. (Cited on page 1)
- Sameer Bibikar, Haris Vikalo, Zhangyang Wang, and Xiaohan Chen. Federated Dynamic Sparse Training: Computing Less, Communicating Less, Yet Learning Better. *Proceedings of the AAAI Conference on Artificial Intelligence*, 36(6):6080–6088, 2022. URL: <https://arxiv.org/abs/2112.09824>. (Cited on page 18)
- Yonatan Bisk, Rowan Zellers, Ronan Le Bras, Jianfeng Gao, and Yejin Choi. PIQA: Reasoning about Physical Commonsense in Natural Language. *CoRR*, abs/1911.11641, 2019. URL: <https://arxiv.org/abs/1911.11641>. (Cited on page 5)
- Leo Breiman. Bagging predictors. *Machine Learning*, 24(2):123–140, 8 1996. ISSN 0885-6125. URL: <https://link.springer.com/article/10.1007/BF00058655>. (Cited on page 1)
- Cerebras. Sparsity Made Easy – Introducing the Cerebras PyTorch Sparsity Library - Cerebras, 2024. URL: <https://www.cerebras.ai/blog/sparsity-made-easy-introducing-the-cerebras-pytorch-sparsity-library> [Accessed: 25.04.2025]. (Cited on page 8, 26)
- Christopher Clark, Kenton Lee, Ming-Wei Chang, Tom Kwiatkowski, Michael Collins, and Kristina Toutanova. BoolQ: Exploring the Surprising Difficulty of Natural Yes/No Questions. *CoRR*, abs/1905.10044, 2019. URL: <https://arxiv.org/abs/1905.10044>. (Cited on page 5)
- Peter Clark, Isaac Cowhey, Oren Etzioni, Tushar Khot, Ashish Sabharwal, Carissa Schoenick, and Oyvind Tafjord. Think you have Solved Question Answering? Try ARC, the AI2 Reasoning Challenge. *CoRR*, abs/1803.05457, 2018. URL: <https://arxiv.org/abs/1803.05457>. (Cited on page 5)
- Selima Curci, Decebal Constantin Mocanu, and Mykola Pechenizkiy. Truly Sparse Neural Networks at Scale. 2021. URL: <https://arxiv.org/abs/2102.01732>. (Cited on page 26)
- Jia Deng, Wei Dong, Richard Socher, Li-Jia Li, Kai Li, and Li Fei-Fei. ImageNet: A large-scale hierarchical image database. In *2009 IEEE Conference on Computer Vision and Pattern Recognition*, pages 248–255. IEEE, 2009. URL: <https://ieeexplore.ieee.org/document/5206848>. (Cited on page 18, 19)
- Tim Dettmers and Luke Zettlemoyer. Sparse Networks from Scratch: Faster Training without Losing Performance, 2019. URL: <https://arxiv.org/abs/1907.04840>. (Cited on page 19)
- Thomas G. Dietterich. Ensemble Methods in Machine Learning. In *Multiple Classifier Systems*, pages 1–15. Springer Berlin Heidelberg, 2000. ISBN 978-3-540-45014-6. URL: [https://link.springer.com/chapter/10.1007/3-540-45014-9\\_1](https://link.springer.com/chapter/10.1007/3-540-45014-9_1). (Cited on page 2)

- Utku Evci, Trevor Gale, Jacob Menick, Pablo Samuel Castro, and Erich Elsen. Rigging the Lottery: Making All Tickets Winners. In *International Conference on Machine Learning*, pages 2943–2952. PMLR, 2020. URL: <https://arxiv.org/abs/1911.11134>. (Cited on page 2, 3, 4, 17, 18, 21, 23)
- Utku Evci, Yani Ioannou, Cem Keskin, and Yann Dauphin. Gradient flow in sparse Neural Networks and how Lottery Tickets win. *Proc. Conf. AAAI Artif. Intell.*, 36(6):6577–6586, June 2022. URL: <https://arxiv.org/abs/2010.03533>. (Cited on page 17, 18)
- William Fedus, Barret Zoph, and Noam Shazeer. Switch Transformers: Scaling to Trillion Parameter Models with Simple and Efficient Sparsity. *Journal of Machine Learning Research*, 2021. URL: <https://arxiv.org/abs/2101.03961>. (Cited on page 16)
- Stanislav Fort, Huiyi Hu, and Balaji Lakshminarayanan. Deep Ensembles: A Loss Landscape Perspective, 2020. URL: <https://arxiv.org/abs/1912.02757>. (Cited on page 2)
- Jonathan Frankle and Michael Carbin. The Lottery Ticket Hypothesis: Training Pruned Neural Networks. *International Conference on Learning Representations*, 2019. URL: <https://arxiv.org/abs/1803.03635>. (Cited on page 2, 3, 17)
- Yoav Freund and Robert E Schapire. A Decision-Theoretic Generalization of On-Line Learning and an Application to Boosting. *Journal of Computer and System Sciences*, 55(1):119–139, 1997. URL: <https://www.sciencedirect.com/science/article/pii/S002200009791504X>. (Cited on page 1)
- Heitor Murilo Gomes, Jean Paul Barddal, Fabrício Enembreck, and Albert Bifet. A Survey on Ensemble Learning for Data Stream Classification. *ACM Computing Surveys*, 50(2):1–36, March 2017. ISSN 1557-7341. URL: <https://dl.acm.org/doi/10.1145/3054925>. (Cited on page 2)
- Laura Graesser, Utku Evci, Erich Elsen, and Pablo Samuel Castro. The State of Sparse Training in Deep Reinforcement Learning. In *International Conference on Machine Learning*, pages 7766–7792. PMLR, 2022. URL: <https://arxiv.org/abs/2206.10369>. (Cited on page 18)
- Bram Grooten, Ghada Sokar, Shibhansh Dohare, Elena Mocanu, Matthew E. Taylor, Mykola Pechenizkiy, and Decebal Constantin Mocanu. Automatic Noise Filtering with Dynamic Sparse Training in Deep Reinforcement Learning. *Int. Conf. Autonomous Agents and Multiagent Systems (AAMAS)*, 2023. URL: <https://arxiv.org/abs/2302.06548>. (Cited on page 18)
- Chuan Guo, Geoff Pleiss, Yu Sun, and Kilian Q Weinberger. On Calibration of Modern Neural Networks. In *International Conference on Machine Learning*, pages 1321–1330. PMLR, 2017. URL: <https://proceedings.mlr.press/v70/guo17a.html>. (Cited on page 23)
- Song Han, Jeff Pool, John Tran, and William J. Dally. Learning both Weights and Connections for Efficient Neural Networks. *Advances in Neural Information Processing Systems*, 2015. URL: <https://arxiv.org/abs/1506.02626>. (Cited on page 3)
- Lars Kai Hansen and Peter Salamon. Neural Network Ensembles. *IEEE Transactions on Pattern Analysis and Machine Intelligence*, 12(10):993–1001, 1990. URL: <https://ieeexplore.ieee.org/document/58871>. (Cited on page 2)
- Trevor Hastie, Robert Tibshirani, and Jerome Friedman. *The Elements of Statistical Learning*. Springer Series in Statistics. Springer New York Inc., 2001. URL: <https://link.springer.com/book/10.1007/978-0-387-84858-7>. (Cited on page 23)
- Marton Havasi, Rodolphe Jenatton, Stanislav Fort, Jeremiah Zhe Liu, Jasper Snoek, Balaji Lakshminarayanan, Andrew Mingbo Dai, and Dustin Tran. Training independent subnetworks for robust prediction. In *International Conference on Learning Representations*, 2021. URL: <https://arxiv.org/abs/2010.06610>. (Cited on page 2, 4, 5, 9, 22)
- Kaiming He, Xiangyu Zhang, Shaoqing Ren, and Jian Sun. Deep Residual Learning for Image Recognition. In *Proceedings of the IEEE Conference on Computer Vision and Pattern Recognition*, 2016. URL: <https://arxiv.org/abs/1512.03385>. (Cited on page 9, 18)
- Dan Hendrycks and Thomas Dietterich. Benchmarking Neural Network Robustness to Common Corruptions and Perturbations. In *International Conference on Learning Representations*, 2019. URL: <https://arxiv.org/abs/1903.12261>. (Cited on page 5)
- Dan Hendrycks, Collin Burns, Steven Basart, Andy Zou, Mantas Mazeika, Dawn Song, and Jacob Steinhardt. Measuring Massive Multitask Language Understanding. *International Conference for Learning Representations*, 2021. URL: <https://arxiv.org/abs/2009.03300>. (Cited on page 5)

- Geoffrey Hinton, Oriol Vinyals, and Jeff Dean. Distilling the Knowledge in a Neural Network. *Neural Information Processing Systems (Deep Learning Workshop)*, 2015. URL: <https://arxiv.org/abs/1503.02531>. (Cited on page 2)
- Robert A. Jacobs, Michael I. Jordan, Steven J. Nowlan, and Geoffrey E. Hinton. Adaptive Mixtures of Local Experts. *Neural Computation*, 3(1):79–87, 1991. URL: <https://www.cs.toronto.edu/~fritz/absps/jjnh91.pdf>. (Cited on page 16)
- Alan Jeffares, Tennison Liu, Jonathan Crabbé, and Mihaela van der Schaar. Joint Training of Deep Ensembles Fails Due to Learner Collusion. *Advances in Neural Information Processing Systems*, 2023. URL: <https://arxiv.org/abs/2301.11323>. (Cited on page 19)
- Frederick Jelinek, Robert L. Mercer, Lalit R. Bahl, and James K. Baker. Perplexity-a measure of the difficulty of speech recognition tasks. In *Proceedings of the IEEE Symposium on Speech Recognition*, pages 393–398, 1977. URL: <https://pubs.aip.org/asa/jasa/article/62/S1/S63/642598/Perplexity-a-measure-of-the-difficulty-of-speech>. (Cited on page 23)
- Diederik P Kingma and Jimmy Ba. Adam: A Method for Stochastic Optimization. *International Conference for Learning Representations*, 2015. URL: <https://arxiv.org/abs/1412.6980>. (Cited on page 4)
- Alex Krizhevsky. Learning Multiple Layers of Features from Tiny Images. Technical report, University of Toronto, 2009. URL: <https://www.cs.toronto.edu/~kriz/learning-features-2009-TR.pdf>. (Cited on page 18)
- Ludmila I. Kuncheva and Christopher J. Whitaker. Measures of Diversity in Classifier Ensembles and Their Relationship with the Ensemble Accuracy. *Kluwer Academic Publishers*, 2003. URL: <https://doi.org/10.1023/A:1022859003006>. (Cited on page 7)
- Balaji Lakshminarayanan, Alexander Pritzel, and Charles Blundell. Simple and Scalable Predictive Uncertainty Estimation using Deep Ensembles. *Advances in Neural Information Processing Systems*, 2017. URL: <https://arxiv.org/abs/1612.01474>. (Cited on page 2)
- Ya Le and Xuan S. Yang. Tiny ImageNet Visual Recognition Challenge, 2015. URL: [https://cs231n.stanford.edu/reports/2015/pdfs/yle\\_project.pdf](https://cs231n.stanford.edu/reports/2015/pdfs/yle_project.pdf). (Cited on page 19)
- Yann LeCun, John Denker, and Sara Solla. Optimal Brain Damage. In *Advances in Neural Information Processing Systems*, 1989. URL: [https://proceedings.neurips.cc/paper\\_files/paper/1989/file1e/6c9882bbac1c7093bd25041881277658-Paper.pdf](https://proceedings.neurips.cc/paper_files/paper/1989/file1e/6c9882bbac1c7093bd25041881277658-Paper.pdf). (Cited on page 3)
- Hojung Lee and Jong-Seok Lee. Network Fission Ensembles for Low-Cost Self-Ensembles. 2024. URL: <https://arxiv.org/abs/2408.02301>. (Cited on page 4, 17, 22, 23, 25)
- Namhoon Lee, Thalaiyasingam Ajanthan, and Philip H. S. Torr. SNIP: Single-shot Network Pruning based on Connection Sensitivity. *International Conference on Learning Representations*, 2018. URL: <https://arxiv.org/abs/1810.02340>. (Cited on page 2, 17)
- Stefan Lee, Senthil Purushwalkam, Michael Cogswell, David Crandall, and Dhruv Batra. Why M Heads are Better than One: Training a Diverse Ensemble of Deep Networks, 2015. URL: <https://arxiv.org/abs/1511.06314>. (Cited on page 2, 5, 9)
- Pengxiang Li, Lu Yin, and Shiwei Liu. Mix-LN: Unleashing the Power of Deeper Layers by Combining Pre-LN and Post-LN. *International Conference on Learning Representations*, 2025. URL: <https://arxiv.org/abs/2412.13795>. (Cited on page 19)
- Shiwei Liu, Decebal Constantin Mocanu, Amarsagar Reddy Ramapuram Matavalam, Yulong Pei, and Mykola Pechenizkiy. Sparse evolutionary deep learning with over one million artificial neurons on commodity hardware. *Neural Computing and Applications*, 33:2589–2604, 2021a. URL: <https://link.springer.com/article/10.1007/s00521-020-05136-7>. (Cited on page 26)
- Shiwei Liu, Lu Yin, Decebal Constantin Mocanu, and Mykola Pechenizkiy. Do We Actually Need Dense Over-Parameterization? In-Time Over-Parameterization in Sparse Training. *International Conference on Machine Learning*, 2021b. URL: <https://arxiv.org/abs/2102.02887>. (Cited on page 4, 18, 19, 21)
- Shiwei Liu, Tianlong Chen, Zahra Atashgahi, Xiaohan Chen, Ghada Sokar, Elena Mocanu, Mykola Pechenizkiy, Zhangyang Wang, and Decebal Constantin Mocanu. Deep Ensembling with No Overhead for either Training or Testing: The All-Round Blessings of Dynamic Sparsity. *International Conference on Learning Representations*, 2022. URL: <https://arxiv.org/abs/2106.14568>. (Cited on page 2, 4, 5, 9, 18, 22)

- Shiwei Liu, Tianlong Chen, Xiaohan Chen, Li Shen, Decebal Constantin Mocanu, Zhangyang Wang, and Mykola Pechenizkiy. The Unreasonable Effectiveness of Random Pruning: Return of the Most Naive Baseline for Sparse Training. In *Proceedings of the 11th International Conference on Learning Representations*, 2023. URL: <https://arxiv.org/abs/2202.02643>. (Cited on page 4, 17)
- Richard Maclin and David W. Opitz. Popular Ensemble Methods: An Empirical Study. *Journal of Artificial Intelligence Research*, 11:169–198, 2011. URL: <https://arxiv.org/abs/1106.0257>. (Cited on page 2)
- Todor Mihaylov, Peter Clark, Tushar Khot, and Ashish Sabharwal. Can a Suit of Armor Conduct Electricity? A New Dataset for Open Book Question Answering, 2018. URL: <https://arxiv.org/abs/1809.02789>. (Cited on page 5)
- Decebal Constantin Mocanu, Elena Mocanu, Peter Stone, Phuong H Nguyen, Madeleine Gibescu, and Antonio Liotta. Scalable Training of Artificial Neural Networks with Adaptive Sparse Connectivity inspired by Network Science. *Nature communications*, 9(1):1–12, 2018. URL: <https://arxiv.org/abs/1707.04780>. (Cited on page 2, 3, 4, 17)
- Michael C Mozer and Paul Smolensky. Skeletonization: A Technique for Trimming the Fat from a Network via Relevance Assessment. In D. Touretzky, editor, *Advances in Neural Information Processing Systems*, volume 1. Morgan-Kaufmann, 1988. URL: <https://proceedings.neurips.cc/paper/1988/file/07e1cd7dca89a1678042477183b7ac3f-Paper.pdf>. (Cited on page 3)
- Mahdi Pakdaman Naeini, Gregory F Cooper, and Milos Hauskrecht. Obtaining Well Calibrated Probabilities Using Bayesian Binning. In *Proceedings of the AAAI Conference on Artificial Intelligence*, volume 29, 2015. URL: <https://doi.org/10.1609/aaai.v29i1.9602>. (Cited on page 23)
- NeuralMagic. DeepSparse Inference Engine, 2021. URL: <https://neuralmagic.com/deepsparse>. (Cited on page 8, 26)
- Aleksandra I. Nowak, Bram Grooten, Decebal Constantin Mocanu, and Jacek Tabor. Fantastic Weights and How to Find Them: Where to Prune in Dynamic Sparse Training. *Advances in Neural Information Processing Systems*, 36:55160–55192, 2023. URL: <https://arxiv.org/abs/2306.12230>. (Cited on page 4, 18)
- Aleksandra I. Nowak, Łukasz Gniecki, Filip Szatkowski, and Jacek Tabor. Sparser, Better, Deeper, Stronger: Improving Sparse Training with Exact Orthogonal Initialization. In *Proc. of the 41st International Conference on Machine Learning*, 2024. URL: <https://arxiv.org/abs/2406.01755>. (Cited on page 17)
- NVIDIA. ResNet50 v1.5 for PyTorch, 2024. URL: [https://catalog.ngc.nvidia.com/orgs/nvidia/resources/resnet\\_50\\_v1\\_5\\_for\\_pytorch](https://catalog.ngc.nvidia.com/orgs/nvidia/resources/resnet_50_v1_5_for_pytorch). (Cited on page 19)
- Colin Raffel, Noam Shazeer, Adam Roberts, Katherine Lee, Sharan Narang, Michael Matena, Yanqi Zhou, Wei Li, and Peter J Liu. Exploring the Limits of Transfer Learning with a Unified Text-to-Text Transformer. *Journal of Machine Learning Research*, 21(140):1–67, 2020. URL: <https://jmlr.org/papers/v21/20-074.html>. (Cited on page 5, 19)
- Herbert Robbins and Sutton Monro. A Stochastic Approximation Method. *The Annals of Mathematical Statistics*, 22(3):400–407, 1951. ISSN 00034851. URL: <https://www.columbia.edu/~ww2040/8100F16/RM51.pdf>. (Cited on page 4)
- Keisuke Sakaguchi, Ronan Le Bras, Chandra Bhagavatula, and Yejin Choi. WinoGrande: An Adversarial Winograd Schema Challenge at Scale. 2019. URL: <http://arxiv.org/abs/1907.10641>. (Cited on page 6)
- Erik Schultheis and Rohit Babbar. Towards Memory-Efficient Training for Extremely Large Output Spaces – Learning with 500k Labels on a Single Commodity GPU. In *Joint European Conference on Machine Learning and Knowledge Discovery in Databases*, pages 689–704. Springer, 2023. URL: <https://arxiv.org/abs/2306.03725>. (Cited on page 26)
- David B. Skalak. The Sources of Increased Accuracy for Two Proposed Boosting Algorithms. In *AAAI Conference on Artificial Intelligence*, 1996. URL: <https://citeseerx.ist.psu.edu/document?doi=f8115f79d8b951b71c964fc0401d5a716d516ec>. (Cited on page 7, 23)
- Ghada Sokar, Elena Mocanu, Decebal Constantin Mocanu, Mykola Pechenizkiy, and Peter Stone. Dynamic Sparse Training for Deep Reinforcement Learning. *International Joint Conference on Artificial Intelligence*, 2022. URL: <https://arxiv.org/abs/2106.04217>. (Cited on page 18)
- Yiqin Tan, Pihe Hu, Ling Pan, Jiatai Huang, and Longbo Huang. RLx2: Training a Sparse Deep Reinforcement Learning Model from Scratch. In *The Eleventh International Conference on Learning Representations*, 2023. URL: <https://arxiv.org/abs/2205.15043>. (Cited on page 18)

- Hugo Touvron, Thibaut Lavril, Gautier Izacard, Xavier Martinet, Marie-Anne Lachaux, Timothée Lacroix, Baptiste Rozière, Naman Goyal, Eric Hambro, Faisal Azhar, et al. LLaMA: Open and Efficient Foundation Language Models. 2023. URL: <https://arxiv.org/abs/2302.13971>. (Cited on page 18)
- S. Varrette, H. Cartiaux, S. Peter, E. Kieffer, T. Valette, and A. Ollloh. Management of an Academic HPC & Research Computing Facility: The ULHPC Experience 2.0. In *ACM High Performance Computing and Cluster Technologies*, 2022. URL: <https://doi.org/10.1145/3560442.3560445>. (Cited on page 10)
- Ashish Vaswani, Noam Shazeer, Niki Parmar, Jakob Uszkoreit, Llion Jones, Aidan N. Gomez, Lukasz Kaiser, and Illia Polosukhin. Attention Is All You Need. *Advances in Neural Information Processing Systems*, 2017. URL: <https://arxiv.org/abs/1706.03762>. (Cited on page 9)
- Chaoqi Wang, Guodong Zhang, and Roger Grosse. Picking Winning Tickets Before Training by Preserving Gradient Flow. *International Conference on Learning Representations*, 2020. URL: <https://arxiv.org/abs/2002.07376>. (Cited on page 2)
- Haohan Wang, Songwei Ge, Zachary Lipton, and Eric P Xing. Learning Robust Global Representations by Penalizing Local Predictive Power. In *Neural Information Processing Systems*, 2019. URL: [https://papers.nips.cc/paper\\_files/paper/2019/file/3eefceb8087e964f89c2d59e8a249915-Paper.pdf](https://papers.nips.cc/paper_files/paper/2019/file/3eefceb8087e964f89c2d59e8a249915-Paper.pdf). (Cited on page 5)
- Yeming Wen, Dustin Tran, and Jimmy Ba. BatchEnsemble: An Alternative Approach to Efficient Ensemble and Lifelong Learning. *International Conference on Learning Representations*, 2020. URL: <https://arxiv.org/abs/2002.06715>. (Cited on page 2, 5, 9)
- Wieger Wesselink, Bram Grooten, Qiao Xiao, Cassio de Campos, and Mykola Pechenizkiy. Nerva: a Truly Sparse Implementation of Neural Networks. *arXiv preprint arXiv:2407.17437*, 2024. URL: <https://arxiv.org/abs/2407.17437>. (Cited on page 26)
- Tim Whitaker and Darrell Whitley. Prune and Tune Ensembles: Low-Cost Ensemble Learning with Sparse Independent Subnetworks. In *AAAI*, pages 8638–8646. AAAI Press, 2022. ISBN 978-1-57735-876-3. URL: <https://arxiv.org/abs/2202.11782>. (Cited on page 2)
- Thomas Wolf, Lysandre Debut, Victor Sanh, Julien Chaumond, Clement Delangue, Anthony Moi, Pierric Cistac, Tim Rault, Rémi Louf, Morgan Funtowicz, et al. HuggingFace’s Transformers: State-of-the-art Natural Language Processing. 2019. URL: <https://arxiv.org/abs/1910.03771>. (Cited on page 18, 19)
- David H. Wolpert. Stacked generalization. *Neural Networks*, 5(2):241–259, 1992. URL: <https://www.sciencedirect.com/science/article/abs/pii/S08933608005800231>. (Cited on page 1)
- Boqian Wu, Qiao Xiao, Shunxin Wang, Nicola Strisciuglio, Mykola Pechenizkiy, Maurice van Keulen, Decebal Constantin Mocanu, and Elena Mocanu. Dynamic Sparse Training versus Dense Training: The Unexpected Winner in Image Corruption Robustness. *International Conference on Learning Representations*, 2025. URL: <https://arxiv.org/abs/2410.03030>. (Cited on page 5)
- Murat Onur Yildirim, Elif Ceren Gok Yildirim, Ghada Sokar, Decebal Constantin Mocanu, and Joaquin Vanschoren. Continual Learning with Dynamic Sparse Training: Exploring Algorithms for Effective Model Updates. *Conference on Parsimony and Learning*, 2024. URL: <https://arxiv.org/abs/2308.14831>. (Cited on page 18)
- Lu Yin, You Wu, Zhenyu Zhang, Cheng-Yu Hsieh, Yaqing Wang, Yiling Jia, Gen Li, Ajay Jaiswal, Mykola Pechenizkiy, Yi Liang, et al. Outlier Weighed Layerwise Sparsity (OWL): A Missing Secret Sauce for Pruning LLMs to High Sparsity. *International Conference on Machine Learning*, 2023. URL: <https://arxiv.org/abs/2310.05175>. (Cited on page 17)
- Haoran You, Chaojian Li, Pengfei Xu, Yonggan Fu, Yue Wang, Xiaohan Chen, Richard G. Baraniuk, Zhangyang Wang, and Yingyan Lin. Drawing Early-Bird Tickets: Towards More Efficient Training of Deep Networks. *International Conference on Learning Representations*, 2020. URL: <https://arxiv.org/abs/1909.11957>. (Cited on page 17)
- Geng Yuan, Xiaolong Ma, Wei Niu, Zhengang Li, Zhenglun Kong, Ning Liu, Yifan Gong, Zheng Zhan, Chaoyang He, Qing Jin, Siyue Wang, Minghai Qin, Bin Ren, Yanzhi Wang, Sijia Liu, and Xue Lin. MEST: Accurate and Fast Memory-Economic Sparse Training Framework on the Edge. In *Advances in Neural Information Processing Systems*, 2021. URL: <https://arxiv.org/abs/2110.14032>. (Cited on page 18)
- Sergey Zagoruyko and Nikos Komodakis. Wide Residual Networks. *CoRR*, abs/1605.07146, 2016. URL: <https://arxiv.org/abs/1605.07146>. (Cited on page 18)

- Rowan Zellers, Ari Holtzman, Yonatan Bisk, Ali Farhadi, and Yejin Choi. HellaSwag: Can a Machine Really Finish Your Sentence? *Association for Computational Linguistics*, 2019. URL: <https://arxiv.org/abs/1905.07830>. (Cited on page 5)
- Yingtao Zhang, Jialin Zhao, Wenjing Wu, Ziheng Liao, Umberto Michieli, and Carlo Vittorio Cannistraci. Brain-inspired sparse training enables Transformers and LLMs to perform as fully connected. *arXiv preprint arXiv:2501.19107*, 2025. URL: <https://arxiv.org/abs/2501.19107>. (Cited on page 4)
- Jiawei Zhao, Zhenyu Zhang, Beidi Chen, Zhangyang Wang, Anima Anandkumar, and Yuandong Tian. GaLore: Memory-Efficient LLM Training by Gradient Low-Rank Projection. *International Conference on Machine Learning*, 2024. URL: <https://arxiv.org/abs/2403.03507>. (Cited on page 19)
- Rui Zheng, Bao Rong, Yuhao Zhou, Di Liang, Sirui Wang, Wei Wu, Tao Gui, Qi Zhang, and Xuanjing Huang. Robust Lottery Tickets for Pre-trained Language Models. In *Association for Computational Linguistics*, page 2211–2224, 2022. URL: <https://arxiv.org/abs/2211.03013>. (Cited on page 17)
- Zhi-Hua Zhou. *Ensemble Methods: Foundations and Algorithms*. Chapman & Hall/CRC press, 2012. URL: <https://dl.acm.org/doi/10.5555/2381019>. (Cited on page 2)

## Appendix

### Table of Contents

<b>Societal Impact</b>	<b>16</b>
<b>Extended Background and Related Work</b>	<b>16</b>
Ensembling Methods	16
Sparsity	17
<b>Model Architectures</b>	<b>18</b>
<b>Datasets</b>	<b>18</b>
CIFAR-100	18
ImageNet	18
Tiny-ImageNet	18
Colossal Clean Crawled Corpus (C4)	19
<b>Training Settings and Hyperparameters</b>	<b>19</b>
Code	19
Hyperparameters	19
Training Schedules	21
<b>Metrics</b>	<b>23</b>
<b>NeuroTrails Algorithm</b>	<b>24</b>
<b>Additional Results</b>	<b>24</b>
Parameter-Matched Baseline Study	24
Tiny-ImageNet	25
<b>Sparsity Ratio Analysis</b>	<b>25</b>
Ultra Sparse	26
<b>Real-time Inference Gain</b>	<b>26</b>
<b>Goldilocks Image Breakdown</b>	<b>27</b>

## A Societal Impact

This work advances core machine learning capabilities by improving the efficiency and performance of neural networks. While we focus on algorithmic improvements, we acknowledge that, like most technical advances in ML, this work may have various societal impacts. We encourage thoughtful consideration of these implications when building upon this research.

By reducing parameter counts and inference FLOPs, NeuroTrails enables more efficient neural networks that are easier to deploy in resource-constrained environments. These improvements help lower computational overhead and support broader, more sustainable use of AI technologies, especially as hardware increasingly catches up to exploit the use of unstructured sparsity.

## B Extended Background and Related Work

### B.1 Ensembling Methods

**Mixture-of-Experts.** Mixture-of-Experts (MoE) models (Jacobs et al., 1991), such as Switch Transformers (Fedus et al., 2021), also attach multiple expert subnetworks to a shared backbone, but their goal is conditional computation. A learned router selects one or a few experts per token, so only a fraction of the heads run on each forward pass; afterward, the router re-weights and merges the

expert outputs. In contrast, NeuroTrails does not need to train a router and simply activates every sparse head. We do not re-merge intermediate activations and aggregate only at the final logits stage. The absence of routing simplifies training, eliminates token-level gating hyperparameters, and ensures deterministic FLOPs, while dynamic sparse heads keep total compute low and enable efficient and parallelizable inference.

**Network Fission Ensembles.** Network Fission Ensembles (NFE) propose an ensemble learning approach that transforms a conventional neural network into a multi-exit structure through weight pruning and balanced weight grouping (Lee and Lee, 2024). A key advantage of NFE is that it does not require widening layers; all gains are made through intricate arranging of existing layers and parameters. NeuroTrails takes a fundamentally different approach. Our method strategically initializes independent copies of specific network layers into a multi-head structure, followed by sparsification and dynamic topology update. This approach more closely resembles traditional ensemble architectures in its behavior.

## B.2 Sparsity

**Lottery Ticket Hypothesis.** There exists a family of sparsification methods based on the Lottery Ticket Hypothesis (Frankle and Carbin, 2019), which stipulates that each randomly initialized network already contains a subnetwork that can be as accurate as the full network when trained in isolation. Search of this subnetwork through Iterative Magnitude Pruning (IMP) involves training the dense network, pruning  $p$  fraction of weights based on magnitude, and resetting weights to their initial states (excluding the already pruned parameters). Subsequent works have refined and significantly improved this process (Zheng et al., 2022; Bai et al., 2022; You et al., 2020).

**Layerwise Sparsity Ratios.** The distribution of sparsity over the layers of the network is shown to be a vital factor for sparse training procedures (Liu et al., 2023; Yin et al., 2023). The main approaches are:

- Uniform: each layer is assigned the sparsity ratio  $S$ , equal to the global sparsity ratio.
- Erdős–Rényi (ER): this approach (Mocanu et al., 2018) assigns higher sparsities to larger layers. A layer  $l$  of size  $n^{l-1} \times n^l$  receives a sparsity ratio that scales with

$$1 - \frac{n^{l-1} + n^l}{n^{l-1} \cdot n^l}.$$

- Erdős–Rényi–Kernel (ERK): this adaptation of ER is specifically designed by Evci et al. (2020) for convolutional layers, which consists of additional kernel dimensions. The calculation becomes

$$1 - \frac{n^{l-1} + n^l + w^l + h^l}{n^{l-1} \cdot n^l \cdot w^l \cdot h^l}.$$

In all experiments we allocate sparsity with ER; for convolutional layers we switch to its ERK variant. Some other sparse initialization methods involve loss function sensitivity initialization (Lee et al., 2018) or globally random allocations (Liu et al., 2023).

**Static Sparse Training.** Static methods train neural networks with a fixed sparse topology throughout the entire training process. While static sparse training requires fewer FLOPs compared to dense methods, it suffers from several fundamental limitations. The fixed topology prevents the network from adapting its structure during training, making the method highly sensitive to its initialization. This rigidity can create suboptimal paths for gradient flow and potentially limit the learning capacity of the network (Evci et al., 2022). There are promising directions to overcome these challenges (Nowak et al., 2024). Despite its limitations, static sparse training remains an important simple baseline in the sparse training field.

**Dynamic Sparse Training.** Methods in the domain of DST involve models that begin with sparse architectures and dynamically adapt their network topology during training. This process enables the network to explore alternative topologies in an evolutionary manner, gradually discovering more optimal network structures during training. SET (Mocanu et al., 2018), described in Section 2, has

been successfully applied in different domains, from unsupervised and supervised learning (Nowak et al., 2023; Liu et al., 2021b, 2022; Yuan et al., 2021), to reinforcement learning (Grooten et al., 2023; Sokar et al., 2022) and continual learning (Yildirim et al., 2024). RigL (Evci et al., 2020) has also been widely adopted in research, having been applied in supervised learning (Nowak et al., 2023; Evci et al., 2022), reinforcement learning (Graesser et al., 2022; Tan et al., 2023), federated learning (Bibikar et al., 2022), and others. In a related line of work, Bellec et al. (2017) proposed DeepR, a similar approach where weights are pruned whenever the optimizer flips their sign, i.e., when weights are close to zero.

## C Model Architectures

**ResNet-50** is a 50-layer deep convolutional neural network that introduced the concept of residual learning to address the vanishing gradient problem in deep networks (He et al., 2016). It uses skip connections (or shortcuts) to bypass one or more layers, enabling the training of very deep networks by allowing gradients to flow directly through these connections. Its architecture consists of a series of residual blocks, each containing multiple convolutional layers and batch normalization layers.

**Wide Residual Networks** such as Wide-ResNet28-10 are an extension of the original ResNets that focus on increasing the width (number of filters) of residual layers rather than their depth (Zagoruyko and Komodakis, 2016). This approach has been shown to improve performance while reducing computational complexity compared to very deep ResNets. Wide-ResNet achieves this by using fewer layers but with more convolutional filters per layer, which enhances feature learning and generalization.

**LLaMA-130M** and **LLaMA-350M** are members of the decoder-only LLaMA family introduced by Touvron et al. (2023). The smaller variant comprises 12 transformer blocks with 768-dimensional hidden states and 12 attention heads, while the larger consists of 24 transformer blocks with 1024-dimensional hidden states and 16 attention heads. Both models retain the architectural choices of their larger counterparts, with LLaMA-130M fitting on commodity GPUs and achieving competitive perplexity for its size, serving as a strong lightweight backbone for further language-model experiments. LLaMA-350M offers greater capacity while maintaining the core architectural principles of the series. Our implementation of both models employs the open-source HuggingFace reproduction of LLaMA (Wolf et al., 2019).

## D Datasets

### D.1 CIFAR-100

CIFAR-100 is an image classification dataset consisting of 60,000 color images sized 32×32 pixels, divided into 100 classes with 600 images per class. The dataset is split into 50,000 training and 10,000 test images (Krizhevsky, 2009).

**License:** CIFAR-100 is available for academic research and is distributed under the MIT License.

### D.2 ImageNet

ImageNet is a large-scale, high-resolution image database designed for research in visual object recognition. It contains over 14 million annotated images. The dataset has been foundational for advances in deep learning and computer vision, particularly through the ImageNet Large Scale Visual Recognition Challenge (ILSVRC), which includes 1,281,167 training images, 50,000 validation images, and 100,000 test images across 1,000 object categories (Deng et al., 2009).

**License:** ImageNet is available for non-commercial research and educational purposes under a custom non-commercial license. Access requires agreement to ImageNet terms of use, which restrict commercial exploitation.

### D.3 Tiny-ImageNet

Tiny-ImageNet is a subset of the full ImageNet dataset, containing 100,000 images of size 64×64 pixels, labeled across 200 classes. Each class has 500 training images, 50 validation images, and 50

test images, making it suitable for experiments requiring a smaller-scale version of ImageNet (Le and Yang, 2015; Deng et al., 2009).

**License:** Tiny-ImageNet is distributed for academic and research purposes only, under the same non-commercial terms as ImageNet.

#### D.4 Colossal Clean Crawled Corpus (C4)

C4 is a large-scale text dataset constructed by cleaning and filtering web-crawled data from Common Crawl. It contains hundreds of gigabytes of English text, designed for training large language models and other NLP tasks. The dataset is filtered to remove low-quality and non-English content (Raffel et al., 2020).

**License:** The C4 dataset is used under the Open Data Commons Attribution License (ODC-By) v1.0, which allows free sharing, creation, and adaptation of the database provided proper attribution is maintained.

### E Training Settings and Hyperparameters

#### E.1 Code

For computer vision experiments, we built upon the codebases from Liu et al. (2021b) and Dettmers and Zettlemoyer (2019), implementing our method throughout their existing sparse training library. The codebase from Dettmers and Zettlemoyer (2019) is released under the MIT license.

For language experiments, we used the codebases from Li et al. (2025) and Zhao et al. (2024) as a foundation, implementing NeuroTrails in conjunction with their LLaMA architectures based on HuggingFace’s reproduction (Wolf et al., 2019). The codebase from Zhao et al. (2024) is licensed under Apache 2.0.

#### E.2 Hyperparameters

In this section, we describe the hyperparameters for our experiments. See Tables 9 and 10 for the settings of our computer vision and language experiments, respectively.

**Computer Vision.** For CIFAR-100 and Tiny-ImageNet we train Wide-ResNet28-10 using SGD with momentum 0.9 and an initial learning rate of 0.1. The batch size is 128, the L2 regularization constant is set to 0.0005. For ImageNet, we follow the standard training regime (NVIDIA, 2024). We train ResNet-50 using SGD with a momentum of 0.875 and an initial learning rate of 0.256. The batch size is set to 256. We use L2 regularization with a fixed constant of  $3.05e-05$ . For all computer vision datasets, the learning rate decreases by a factor of 10 after 25%, 50%, and 75% of training.

Dynamic sparse training hyperparameters are set as follows: pruning and regrowing 50% of the available parameters (promoting a high degree of topology adjustment) at the beginning, with a cosine decay to 0 by the last training epoch. The  $\Delta T$  topology update interval is set to 100 for CIFAR-100 and 1000 for ImageNet.

For the static sparse baseline of Section 5.1, we instantiate the model with the desired sparsity ratio at the start and subsequently train without adjusting the topology. For the pruning baseline, we employ global magnitude pruning to achieve the target sparsity ratio after the first 50% of training. After reaching the desired sparsity, we fine-tune the model for the remaining duration without making any further changes to its topology.

For ensemble training, we use the independent training paradigm, shown to work well by Jeffares et al. (2023), and train networks separately. At test time, we gather each network’s predictions for the batch and average their raw probabilities, i.e., soft voting.

**Language Modeling.** For our language modeling experiments on the C4 corpus with LLaMA-130M/350M, we present the hyperparameters in Table 10. We train with Adam using a learning rate cosine-decay schedule (minimum LR set to 10% of the base) and a linear warmup over the first 10% of update steps. The batch size is 512 tokens, and we run on four A100 GPUs.

Table 9: Hyperparameters and settings for **computer vision** experiments.

Parameter	Value
<i>Shared by all experiments</i>	
optimizer	SGD with momentum (see below)
learning rate schedule	0.1× step decay at 25%, 50%, 75% of training
ensemble aggregation	soft voting (mean of probabilities)
<i>CIFAR-100 and Tiny-ImageNet</i> (all baselines)	
model	Wide-ResNet28-10
momentum	0.9
initial learning rate	0.1
batch size	128
weight decay (L2)	$5 \cdot 10^{-4}$
training device	1 × NVIDIA V100 (16GB memory) - CIFAR-100 4 × NVIDIA A100 (40GB memory) - Tiny-ImageNet
approx. training time	6.25h (CIFAR-100), 5.41h (Tiny-ImageNet)
<i>ImageNet</i> (all baselines)	
model	ResNet-50
momentum	0.875
initial learning rate	0.256
batch size	256
weight decay (L2)	$3.05 \cdot 10^{-5}$
training device	4 × NVIDIA A100 (40GB memory)
approx. training time	53h
<i>Static Sparse baseline</i>	
sparsity ratio	varying (Section 5.1)
sparsity initialization	ER
topology update interval ( $\Delta T$ )	$\infty$ (no change)
<i>NeuroTrails</i>	
sparsity ratio	varying (Section 4)
sparsity initialization	ER
DST drop fraction	$0.5 \cdot \text{cosine\_decay}(t)$
DST grow method	gradient (RigL)
DST prune method	magnitude-based
topology update interval ( $\Delta T$ )	100 (CIFAR-100), 1000 (ImageNet)
blocks in head	8 (CIFAR-100), 10 (ImageNet)
<i>Pruning baseline</i>	
sparsity ratio	varying (Section 5.1)
pruning method	global magnitude
pre-pruning phase	250 epochs
fine-tuning phase	250 epochs
<i>TreeNet</i>	
blocks in head	8 (CIFAR-100), 10 (ImageNet)
<i>Full Ensemble</i>	
training paradigm	Independent training

Table 10: Hyperparameters and settings for **language modeling** experiments.

Parameter	Value
<i>Shared by all experiments</i>	
model size	130M, 350M
optimizer	Adam
learning rate	$1.5e - 3$ for 130M, $5e - 4$ for 350M
learning rate schedule	cosine decay (min LR: $0.1 \times \text{base}$ ) + warmup
learning rate warmup	10% of update steps
weight decay	0 (no decay)
ensemble aggregation	soft voting (mean of probabilities)
batch size	512
vocabulary size	32,000
max sequence length	1024
data type	bfloat16
training device	$4 \times \text{NVIDIA A100 (40GB memory)}$
approx. training time	7.5h (130M), 40h (350M)
<i>NeuroTrails</i>	
sparsity ratio	0.1
sparsity initialization	ER with attention projections dense
DST drop fraction	$0.5 \cdot \text{cosine\_decay}(t)$
DST grow method	gradient (RigL)
DST prune method	soft magnitude
soft magnitude temperature	3.0
topology update interval ( $\Delta T$ )	50 steps
blocks in head	8 (130M), 16 (350M)
<i>TreeNet</i>	
blocks in head	8 (130M), 16 (350M)
<i>Full Ensemble</i>	
training paradigm	Independent training

Our NeuroTrails models employ dynamic sparse training: at every  $\Delta T = 50$  steps we drop and regrow a fraction  $p$  of the weights, decaying the drop fraction to zero by the end of training. We allocate 8 or 16 transformer blocks per head, matching the approximate  $1/3$  shared-backbone setting used in our vision experiments. This configuration lets each head discover and adapt its own topology while respecting the overall FLOP budget.

As a reference, we split the TreeNet baseline likewise into a shared backbone and 8 or 16-block heads. For the dense-ensemble baseline, we train three independent LLaMA-130M models from scratch under the same schedule and aggregate their outputs via the same soft-voting scheme.

Experiments on C4, ImageNet, and Tiny-ImageNet have been carried out using distributed training on 4 NVIDIA A100 GPUs, while for CIFAR-100 training was done on a single NVIDIA V100.

### E.3 Training Schedules

Building on the observation that dense models tend to overfit once training is prolonged, whereas sparse networks keep improving as they are still refining both weights and topology (Liu et al., 2021b), we follow the recipe of Evci et al. (2020) and extend the training of sparse variants by at most  $1/(1-S)$ , so that its total FLOPs never exceeds that of the dense counterpart. Exact training schedules appear in Tables 11 to 14.

In Table 11 we report the number of epochs and relative training FLOPs on CIFAR-100 with Wide-ResNet28-10. The dense model runs for 250 epochs (3.6e17 FLOPs). Sparse methods such as EDST ( $S = 0.9$ ) and DST ( $S = 0.8$ ) run up to 850 or 750 total epochs—to compensate for their reduced per-epoch cost, while other baselines (MIMO, BatchEnsemble, NFE, TreeNet) stay close to 250. NeuroTrails is trained for 450 epochs, calibrated to maintain computational efficiency significantly below a single dense network, as measured by total training FLOPs.

Table 11: Training cost comparison on CIFAR-100 (Wide-ResNet28-10). Baselines marked with \* are from Havasi et al. (2021), \*\* from Liu et al. (2022), and \*\*\* from Lee and Lee (2024).

Name	Train Epochs	Train FLOPs ( $\downarrow$ )
Single Dense *	250	3.6e17
MIMO ( $M = 3$ ) *	250	1.00×
EDST Ensemble ( $M = 7$ ) ( $S = 0.9$ ) **	850	0.57×
DST Ensemble ( $M = 3$ ) ( $S = 0.8$ ) **	3×250	1.01×
Batch Ensemble ( $M = 4$ ) *	250	1.10×
NFE ( $M = 3$ ) ***	200	1.02×
TreeNet ( $M = 3$ )	250	2.91×
Full Ensemble ( $M = 3$ )	3×250	3.00×
NeuroTrails ( $M = 3$ ) ( $S = 0.8$ )	450	0.85×
NeuroTrails ( $M = 5$ ) ( $S = 0.9$ )	450	0.67×

Table 12 shows the analogous schedule on ImageNet (ResNet-50). The single-model baseline uses 90 epochs (4.8e18 FLOPs); EDST and DST extend to 310 and 400 total epochs respectively, whereas NeuroTrails ( $S = 0.7$ ) runs for 270 epochs—staying close to a single dense model’s compute budget. Notably, most baselines tune their schedules so that total training FLOPs remain close to the 1.0× dense reference. We recognize that reported training lengths vary substantially across papers; to ensure fidelity to each comparison, we simply report each method’s published schedule when taking values from the original works. We encourage the ensembling field to always publish the full training schedules of all baselines and adopt more consistent training protocols, to enable clearer comparisons.

Table 12: Training cost comparison on ImageNet (ResNet-50). Baselines marked with \* are from Havasi et al. (2021), \*\* from Liu et al. (2022).

Name	Train Epochs	Train FLOPs ( $\downarrow$ )
Single Dense *	90	4.8e18
MIMO ( $M = 2$ ) ( $\rho = 0.6$ ) *	150	1.00×
EDST Ensemble ( $M = 4$ ) ( $S = 0.8$ ) **	310	0.87×
DST Ensemble ( $M = 2$ ) ( $S = 0.8$ ) **	2×200	1.12×
Batch Ensemble ( $M = 4$ ) *	4×135	1.10×
TreeNet ( $M = 3$ )	180	2.91×
Full Ensemble ( $M = 4$ ) *	4×90	4.00×
NeuroTrails ( $M = 3$ ) ( $S = 0.7$ )	270	1.10×

For C4 pretraining with LLaMA models, Table 13 compares the number of weight-update steps, total tokens seen, and training FLOPs across different methods. The dense baseline for LLaMA-130M performs 10,000 updates (1.0B tokens), while NeuroTrails ( $S = 0.1$ ) scales to 11,111 steps (1.1B tokens), precisely matching TreeNet’s training FLOPs via the  $1/(1-S)$  rule. A similar scaling applies to the larger LLaMA-350M model, where NeuroTrails with sparsity 0.1 takes 44,444 steps (4.4B tokens), again equating to the training FLOPs of the dense counterpart.

Table 13: Compute comparison on C4 pretraining (LLaMA-130M/350M).

Name	Train Updates	Tokens seen	Training FLOPs ( $\downarrow$ )
<i>LLaMA-130M</i>			
Single Dense	10,000	1.0B	3.5e18
TreeNet ( $M = 3$ )	10,000	1.0B	2.21×
Full Ensemble ( $M = 3$ )	3×10,000	1.0B	3.00×
NeuroTrails ( $M = 3$ ) ( $S = 0.1$ )	11,111	1.1B	2.21×
<i>LLaMA-350M</i>			
Single Dense	40,000	4.0B	3.5e18
TreeNet ( $M = 3$ )	40,000	4.0B	2.27×
Full Ensemble ( $M = 3$ )	3×40,000	4.0B	3.00×
NeuroTrails ( $M = 3$ ) ( $S = 0.1$ )	44,444	4.4B	2.27×

Finally, Table 14 gives epochs and FLOPs on Tiny-ImageNet (see results in Appendix H). The baseline is 100 epochs (3.2 e17 FLOPs), NFE variants pretrained on CIFAR-100 add a 200-epoch warm-up, and NeuroTrails heads ( $S = 0.8, 0.9$ ) run 200 epochs—staying well below the  $1/(1-S)$  rule—achieving 0.74× training FLOPs compared to a single dense model.

Table 14: Training cost comparison on Tiny-ImageNet (Wide-ResNet28-10). Baselines marked with \* are from Lee and Lee (2024).

Name	Train Epochs	Train FLOPs ( $\downarrow$ )
Single Dense	100	3.2e17
NFE ( $M = 2$ ) ( $S = 0.25$ ) (pretrained on CIFAR-100) *	100(+200 pre)	0.76×
NFE ( $M = 3$ ) ( $S = 0$ ) (pretrained on CIFAR-100) *	100(+200 pre)	1.01×
TreeNet ( $M = 3$ )	100	2.91×
Full Ensemble ( $M = 3$ )	3×100	3.00×
NeuroTrails ( $M = 3$ ) ( $S = 0.8$ )	200	0.94×
NeuroTrails ( $M = 5$ ) ( $S = 0.9$ )	200	0.74×

## F Metrics

**Test Accuracy** quantifies the model’s generalization capability by measuring the proportion of correctly classified samples in a held-out test set (Hastie et al., 2001). Higher test accuracy indicates better classification performance. This fundamental metric serves as the primary indicator of classification quality, though it should be interpreted in conjunction with uncertainty-aware metrics.

**Negative Log-Likelihood (NLL)** (Hastie et al., 2001) evaluates the quality of probabilistic predictions by computing the negative logarithm of predicted probability assigned to the true class, where lower values indicate superior uncertainty estimation.

**Expected Calibration Error (ECE)** (Guo et al., 2017; Naeini et al., 2015) measures the model calibration by calculating the discrepancy between the prediction confidence and the empirical accuracy between different confidence bins. Lower ECE indicates better calibration, meaning the model confidence estimates align more closely with actual accuracy. We used 15 bins to estimate this metric, following (Guo et al., 2017).

**Perplexity** is a statistical measure used to evaluate how well a probabilistic model predicts a sample, commonly applied in natural language processing to assess language models (Jelinek et al., 1977). It quantifies the model’s uncertainty when predicting the next token in a sequence by calculating the exponential of the average negative log-likelihood, with lower perplexity values indicating higher quality models.

**Prediction Disagreement** quantifies the extent to which multiple models produce differing outputs for the same input (Skalak, 1996). Higher disagreement often indicates areas of uncertainty, offering insight into decision boundaries and aiding in the detection of out-of-distribution samples.

**Throughput** for a machine learning model is defined as the number of data samples processed by the model per unit time, typically measured in items or images per second.

**Latency** for a machine learning model is the time taken for the model to process a data sample from input to output, usually measured in milliseconds or seconds per batch.

**FLOPs** refers to the number of floating-point operations a model performs during training or inference. It serves as a measure of the model’s computational complexity and efficiency. We adopt the FLOPs calculation methodology from Evci et al. (2020): For a given dense architecture with forward pass FLOPs  $f_D$  and a sparse version with FLOPs  $f_S$ , the total FLOPs required for one update step scale with  $3 \cdot f_S$  and  $3 \cdot f_D$  FLOPs, respectively. This scaling arises because training consists of two main steps: (1) a forward pass, where activations are computed and stored layer-by-layer to evaluate the loss, and (2) a backward pass, where the error signal is back-propagated to compute gradients. The backward pass is approximately twice as expensive as the forward pass, as each layer must compute gradients with respect to both its parameters *and* its input activations. For further details we refer to Appendix H of the RigL paper (Evci et al., 2020).

## G NeuroTrails Algorithm

The NeuroTrails algorithm, detailed in Algorithm 1, aims to efficiently enhance the performance of neural network ensembles while significantly reducing their parameter footprint. The approach splits a given base architecture into a shared backbone and multiple sparse heads, initializing each part with a target sparsity ratio. Throughout training, each head independently processes shared representations from the backbone, enabling diverse predictions while leveraging common feature extraction.

Periodically, the algorithm dynamically updates the network’s topology through iterative pruning and growing of parameters, controlled by a topology exploration parameter. During inference, predictions from individual heads are combined by averaging their output probabilities, resulting in a final aggregated prediction that leverages the strengths of each sparse pathway. See also Section 3 for further details.

---

### Algorithm 1 NeuroTrails Construction and Operation

---

- 1: **Input:** Base architecture  $\mathcal{F}$ , number of heads  $M$ , splitting block index  $\ell$ , sparsity ratio  $S$ , topology exploration parameter  $p$ .
- 2:
- 3: **Initialization Phase:**
- 4: Split  $\mathcal{F}$  at block  $\ell$  into shared blocks  $\mathcal{F}_s$  and independent heads  $\mathcal{F}_h$
- 5: Initialize  $\mathcal{F}_s$  to sparsity ratio  $S$
- 6: **for** each head  $i \in \{1, \dots, M\}$  **do**
- 7:     Initialize  $\mathcal{F}_h^i$  to sparsity ratio  $S$
- 8: **end for**
- 9:
- 10: **Training Phase:**
- 11: **for** each training iteration **do**
- 12:      $h_s = \mathcal{F}_s(x)$
- 13:     **for** each head  $i \in \{1, \dots, M\}$  **do**
- 14:          $\hat{y}^i = \mathcal{F}_h^i(h_s)$
- 15:          $\mathcal{L}_i = \mathcal{L}(\hat{y}^i, y)$
- 16:     **end for**
- 17:      $\mathcal{L} = \frac{1}{n} \sum_{i=1}^n \mathcal{L}_i$
- 18:      $\theta_e \leftarrow \theta_e - \eta \nabla_{\theta_e} \mathcal{L}$
- 19:     **if** current iteration %  $\Delta T = 0$  **then**
- 20:         Prune  $p$  number of parameters layerwise
- 21:         Grow  $p$  number of parameters layerwise
- 22:     **end if**
- 23: **end for**
- 24:
- 25: **Inference Phase:**
- 26: Compute NeuroTrails prediction  $\hat{y}$  by averaging the class probabilities predicted by each head  $j$ :

$$\hat{y} = \arg \max_i \left( \frac{1}{n} \sum_{j=1}^n \text{softmax } \mathcal{F}_h^j(\mathcal{F}_s(x))_i \right)$$


---

## H Additional Results

### H.1 Parameter-Matched Baseline Study

To isolate the effect of *sparsity + multi-head sharing* from sheer model size, we build a parameter-matched NeuroTrails variant whose total parameter budget is essentially identical to that of a larger dense model. We compare a single dense LLaMA-250M model with a NeuroTrails variant of LLaMA-130M which we designed to match the number of parameters. It uses 3 heads, with just 7 blocks per head (instead of our default 8), and a sparsity ratio of 13%. We train both for exactly the same number of update steps (10k), meaning both models see approximately 1B training tokens. As shown in Table 15, NeuroTrails delivers a modestly lower validation perplexity (26.48 vs. 26.59), despite having slightly fewer parameters than the 250M dense baseline.

Table 15: Size–efficiency comparison: a 250 M-parameter single dense model versus a NeuroTrails variant with essentially the same parameter budget.

Name	Perplexity ( $\downarrow$ )	Parameters ( $\downarrow$ )	Train FLOPs ( $\downarrow$ )	Infer. FLOPs ( $\downarrow$ )
Single Dense	26.59	247.37M	7.0e18	4.56e11
NeuroTrails ( $M = 3, S = 0.13$ )	<b>26.48</b>	245.66M	1.0×	1.0×

## H.2 Tiny-ImageNet

In this section, we present results from training our model on the Tiny-ImageNet benchmark in Table 16. NeuroTrails outperforms the baselines trained from scratch at a competitive accuracy. Furthermore, NeuroTrails requires significantly fewer inference FLOPs than any other model, using only 34% of the budget of a single dense model.

Table 16: Performance on Tiny-ImageNet (Wide-ResNet28-10). NeuroTrails and TreeNet have 8 blocks in the heads, with 4 in the backbone. Results marked with \* are from Lee and Lee (2024), who did not report NLL and ECE, and used a pretrained model instead of training from scratch.

Name	Accuracy ( $\uparrow$ )	NLL ( $\downarrow$ )	ECE ( $\downarrow$ )	Train FLOPs ( $\downarrow$ )	Infer. FLOPs ( $\downarrow$ )
Single Dense	66.5	1.510	0.121	3.2e17	10.5e9
NFE ( $M=2, S=0.25$ ) (pretrained on CIFAR-100) *	<b>71.0</b>	-	-	0.76×	0.76×
NFE ( $M=3, S=0$ ) (pretrained on CIFAR-100) *	70.6	-	-	1.01×	1.01×
TreeNet ( $M = 3$ )	69.6	1.310	0.118	2.91×	2.91×
Full Ensemble ( $M = 3$ )	70.8	1.273	0.115	3.00×	3.00×
NeuroTrails ( $M = 3$ ) ( $S = 0.8$ )	70.7	1.322	0.117	0.94×	0.47×
NeuroTrails ( $M = 5$ ) ( $S = 0.9$ )	70.9	1.251	0.115	<b>0.74×</b>	<b>0.34×</b>

## I Sparsity Ratio Analysis

This section examines the relationship between sparsity ratios and the accuracy of the model. To ensure a controlled analysis, we fix the ensemble size at 3, set the backbone sharing factor to 8, and vary the sparsity ratio from fully dense, which corresponds to being 0% sparse, to 99% sparse.

Our experimental results indicate that for CIFAR-100, optimal performance is achieved at 80% sparsity, where the model retains only 20% of its original parameters (Figure 7). Interestingly, the dense model performs worse, probably due to the overparameterization introduced during the ensemblification process, leading to overfitting. These results underscore the critical role of sparsity as a regularization mechanism in NeuroTrails, which enhances the model’s predictive performance.

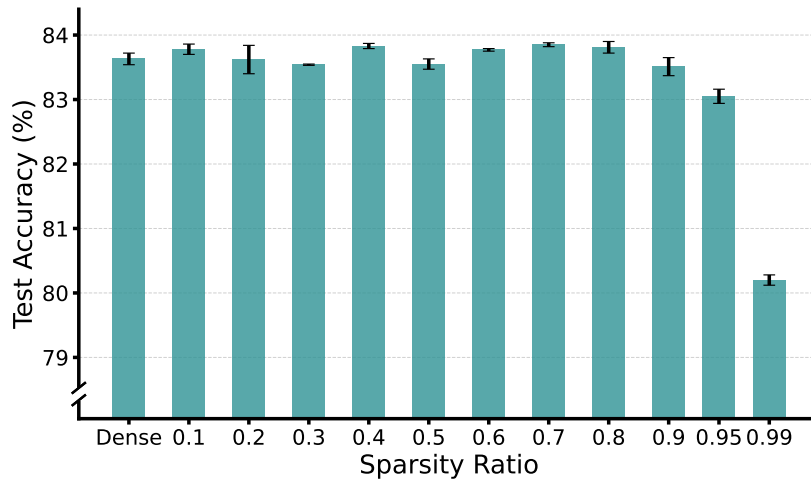


Figure 7: Impact of sparsity ratio on accuracy in a NeuroTrails model with three heads ( $M = 3$ , Wide-ResNet28-10) on CIFAR-100. The 80% sparse configuration emerges as the optimal choice, though the performance differences across closest competitors are notably small.

## I.1 Ultra Sparse

We provide additional experiments with ultra-sparse networks in Table 17. While performance gradually declines with increasing sparsity, models still maintain strong accuracy even in the ultra-sparse regime. These regimes are crucial for real-world deployment, especially on devices with limited computational capacity. We present examples of real-time inference gains in Section 5.4 and Appendix J.

Table 17: NeuroTrails performance in ultra-sparse regimes on CIFAR-100.

Model on CIFAR-100	Accuracy $\uparrow$ (%)
NeuroTrails ( $M = 3$ ) ( $S = 0.95$ )	$83.05 \pm 0.11$
NeuroTrails ( $M = 3$ ) ( $S = 0.99$ )	$80.20 \pm 0.08$
NeuroTrails ( $M = 5$ ) ( $S = 0.95$ )	$83.48 \pm 0.04$
NeuroTrails ( $M = 5$ ) ( $S = 0.99$ )	$81.06 \pm 0.15$
NeuroTrails ( $M = 5$ ) ( $S = 0.995$ )	$79.24 \pm 0.17$

## J Real-time Inference Gain

In this section we examine the discrepancy between theoretical gains from sparsity and the practical speedups achieved on existing hardware. Despite growing interest in sparsity-aware computation, current hardware support remains limited. Notable developments include the DeepSparse library (NeuralMagic, 2021), which offers CPU-level sparse acceleration through an accessible Python library, and dedicated hardware solutions like Cerebras chips (Cerebras, 2024). However, deploying models on Cerebras hardware typically requires proprietary access, which restricts broader experimentation. By contrast, DeepSparse provides an immediate, open solution for evaluating sparse inference performance. There are multiple other works in the direction of truly sparse implementations on GPU hardware (Schultheis and Babbar, 2023; Liu et al., 2021a; Curci et al., 2021; Wesselink et al., 2024).

As illustrated in Figure 8, the theoretical number of sparse FLOPs (shown in blue) decreases substantially with increasing sparsity, dropping well below the latency of a single dense model (indicated by the dashed line) at 80% sparsity model with 3 heads. However, the extent to which these theoretical savings translate into real-world latency reductions is highly dependent on hardware capabilities. In the absence of dedicated sparsity acceleration (yellow), inference latency remains constant across sparsity levels. Partial hardware support through DeepSparse integration (orange), on the other hand, enables meaningful efficiency gains—particularly at ultra-high sparsity levels (e.g., 95–99%). These findings highlight the promise of sparse model execution under current constraints and underscore the need for further research into hardware architectures optimized for sparsity.

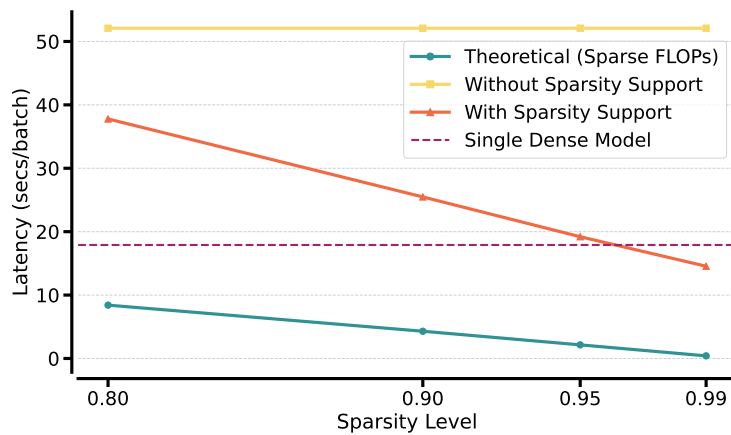


Figure 8: Inference latency comparison across NeuroTrails models with increasing sparsity levels ( $M = 3$ ), using DeepSparse for sparse inference acceleration.

## K Goldilocks Image Breakdown

We defined *prediction conflict* in Section 5.2 and present examples in this section that illustrate this phenomenon. In short, we theorize that models with high prediction diversity among ensemble members may suffer from aggregation inefficiency when these predictions conflict with each other. For the sake of conciness, we refer to model with 8 blocks in head as NeuroTrails 8, and model with 12 blocks in head as NeuroTrails 12 in this section.

This phenomenon is demonstrated in Figure 9, where we observe that the lower prediction disagreement in NeuroTrails 8 consistently produces better prediction estimates, while NeuroTrails 12 exhibits signs of aggregation breakdown, resulting in erroneous predictions. For example, NeuroTrails 8 predicts poppy–poppy–worm for the first image, whereas NeuroTrails 12 predicts orange–sunflower–poppy. The ground truth label is poppy, making the former a correct prediction and the latter an incorrect one. In this instance, the higher prediction diversity in NeuroTrails 12 results in conflicting outputs that hinder accurate aggregation. This illustrates how excessive diversity among predictors can degrade ensemble performance, supporting our hypothesis that prediction conflict undermines aggregation efficiency.

It is important to note that both models achieve high accuracy, with minimal differences between them (83.81% for NeuroTrails 8 versus 83.59% for NeuroTrails 12). While our proposed explanation of prediction conflict may account for this difference, we acknowledge that alternative factors could also contribute to these observations.

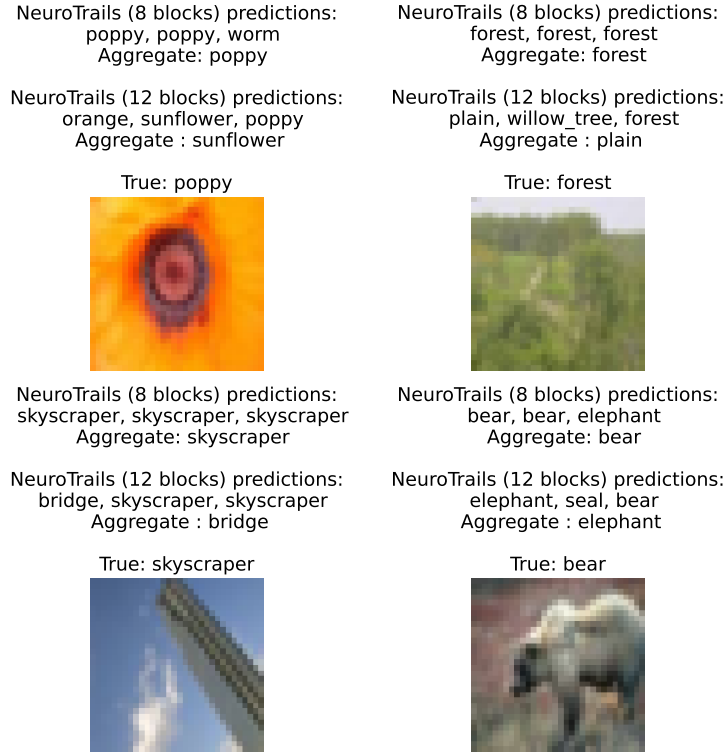


Figure 9: Direct prediction comparison between NeuroTrails models with 8 and 12 blocks in their heads. NeuroTrails-8 exhibits a prediction diversity level that is *just right*, enabling it to produce more accurate results than its counterpart.